Pamukkale Univ Muh Bilim Derg, 31(8), 1469-1493, 2025
(Special Issue of the 10th Geochemistry Symposium)

Pamukkale Üniversitesi Mühendislik Bilimleri Dergisi

Pamukkale University Journal of Engineering Sciences

Mineral chemistry, thermodynamic evolution, and crystallization history of late miocene volcanic rocks around posof (Ardahan, Türkiye)

Posof (Ardahan, Türkiye) civarindaki üst miyosen yaşli volkanik kayaçlarin mineral kimyasi, termodinamik gelişimi ve kristallenme tarihçesi

Derya Cicerali[1*], *Cem Yücel*[2], *Emre Aydınçakır*[1], *Abdullah Kaygusuz*[1]

[1]Department of Geological Engineering, Faculty of Engineering and Natural Sciences, Gümüşhane University, Gümüşhane, Türkiye.
ciceraliderya@gmail.com, aydincakir61@gmail.com, abdullahkaygusuz@gmail.com

[2]Department of Mining Engineering, Faculty of Engineering and Natural Sciences, Gümüşhane University, Gümüşhane, Türkiye.
cemyucel@gumushane.edu.tr

Received/Geliş Tarihi: 29.09.2025 Revision/Düzeltme Tarihi: 29.10.2025 doi: 10.65206/pajes.73473
Accepted/Kabul Tarihi: 30.10.2025 Special Issue Article/Özel Sayı Makalesi

Abstract

This study aimed to constrain the crystallization and emplacement conditions of magmas that produced the Late Miocene volcanic rocks exposed at the junction of the Erzurum-Kars Plateau and the Eastern Pontides in the Northeastern Anatolia Region through a series of thermobarometric analyses. The volcanic succession unconformably overlies Oligocene mudstone, siltstone, and sandstone alternations, with limestone and cherty limestone at higher levels. Petrographically, they consist of fine- to coarse-grained basalt, basaltic andesite, and andesite. Mineral compositions include plagioclase (An_{16-77}), clinopyroxene ($Wo_{39-45}En_{43-50}Fs_{11-12}$), orthopyroxene ($Wo_{3-4}En_{73-82}Fs_{14-24}$), olivine ($Fo_{63-86}$), hornblende (Mg#=0.62-0.79), and Fe-Ti oxides ($Usp_{0.05-1.44}$, $Ilm_{94.10-95.53}$). The groundmass comprises microlites of these minerals and volcanic glass. The dominant textures are microlitic porphyritic, hyalo-microlitic, and microlitic porphyritic, while glomeroporphyritic, intergranular, pilotaxitic, subophitic, flow, and vesicular textures are also observed. Widely present disequilibrium features, such as zoning, sieve, and resorption, are common in plagioclase and clinopyroxene. Thermobarometric calculations indicate crystallization temperatures of 880-1230°C, pressures of 0.73-8.71 kbar, oxygen fugacities between (-10.94) and (-8.92), and water contents of 4.60-6.32 wt.%. These results suggest that the volcanic rocks crystallized under volatile-rich, oxidizing conditions across a broad depth range (~2-32 km), at relatively high temperatures.

Keywords: Late Miocene, Mineral Chemistry, Geothermobarometer, Disequilibrium Crystallization, Posof

Öz

Bu çalışmada, Kuzeydoğu Anadolu Bölgesi'nde Erzurum-Kars Platosu ile Doğu Pontidler'in kesişim noktasında yüzeylenen Üst Miyosen yaşlı volkanik kayaçları oluşturan magmaların kristallenme ve yerleşim koşulları çeşitli termobarometrik hesaplamalar yardımıyla belirlenmiştir. Bu volkanikler Oligosen yaşlı kiltaşı, silttaşı ve kumtaşı ardalanması ile üst seviyelerinde kireçtaşı ve çörtlü kireçtaşlarından oluşan birim üzerine uyumsuz olarak yerleşir. Petrografik olarak; ince iri taneli bazalt, bazaltik andezit ve andezitlerden oluşurlar. Bu kayaçlar; plajiyoklaz (An_{16-77}), klinopiroksen ($Wo_{39-45}En_{43-50}Fs_{11-12}$), ortopiroksen ($Wo_{3-4}En_{73-82}Fs_{14-24}$), olivin ($Fo_{63-86}$), hornblend (Mg#0.62-0.79) ve Fe-Ti oksit ($Usp_{0.05-1.44}$, $İlm_{94.10-95.53}$) minerallerinden ibarettir. Kayaç hamuru tüm bu minerallerin mikrolitleri ve volkan camından meydana gelir. Mikrolitik porfirik, hyalo-mikrolitik ve mikrolitik porfirik doku genel dokuyu oluştururken, glomeroporfirik, intergranüler, pilotaksitik, subofitik, akma ve vesiküler dokular özel dokuları oluşturur. Plajiyoklaz ve klinopiroksenlerde gözlenen zonlanma, elek ve kemirilme dokuları dengesizlik dokulardır. Termobarometrik hesaplamalara göre volkanik kayaçların kristallenme sıcaklıkları 880-1230°C, basınçları 0.73-8.71 kbar, oksijen fugasitesi (-10.94) ile (-8.92) arasında ve su içeriği % 4.60-6.32 arasında değişmektedir. Sonuç olarak incelenen volkanik kayaçların; uçucularca zengin, yüksek oksidasyon koşullarında sığ ile derin kabuksal derinliklerde yüksek sıcaklıklarda (~2–32 km) oluştuğu söylenebilir.

Anahtar kelimeler: Üst Miyosen, Mineral Kimyası Jeotermobarometre, Dengesiz Kristallenme, Posof

1 Introduction

The textural and chemical characteristics of minerals in volcanic and plutonic rocks, bearing diverse geochemical features, have been extensively studied over the past few decades. The magma chamber processes, such as magma mixing, recharge, crystal mush remobilization, fractional crystallization, and assimilation as open and/or closed systems, significantly affect the evolution of the magmas. In particular, the variation in chemical composition and thermodynamic conditions as open system processes leads to disequilibrium during the crustal evolution of the magmas, resulting in zoning, embayment, corrosion, and sieved texture [1]-[3]. The investigation on the petrographic, textural, and mineral chemical properties of the magmas helps us to better understand the magmatic processes [4]-[8]. Furthermore, the physicochemical parameters such as pressure, temperature, oxygen fugacity, and hygrometers can be obtained by using the composition of minerals such as clinopyroxene, amphibole, biotite, feldspar, olivine, and Fe–Ti oxides [9],[10]. These parameters also provide insight into the emplacement/storage depth and thermal evolution of magmas. In the last four decades, many thermobarometric calibrations based on the mineral and melt composition, which is in equilibrium with it, have been proposed by many researchers [11]-[20]. By using these parameters, it is possible to shed light on the evolution and crystallization history of the magma during the crustal movement.

*Corresponding author/Yazışılan Yazar

In this study, we present the new textural features and mineral chemistry dataset of diverse minerals, such as orthopyroxene, clinopyroxene, plagioclase, and hornblende from the studied Late Miocene basic volcanic rocks from the Posof vicinity (Ardahan, Türkiye). We use these features to put forward the following objectives: (i) determine petrographic features; (ii) carry out thermodynamic conditions in terms of intensive parameters (P, T, and fO_2) to identify emplacement and pre-eruptive crystallization history; (iii) understand magma chamber processes based on the strength and composition of deep-, mid-, and shallow-continental crusts.

2 Regional geology

The study area is in the intersection of the Eastern Pontides orogenic belt, which is in the central part of the Alpine-Himalayan orogenic belt, and is of key importance to understand the tectono-magmatic evolution of the Alpine system, and the Eastern Anatolian, which is one of the best places for collision-related volcanism in the world. The five different tectonic blocks were identified according to their tectonic and geological properties (Figure 1).

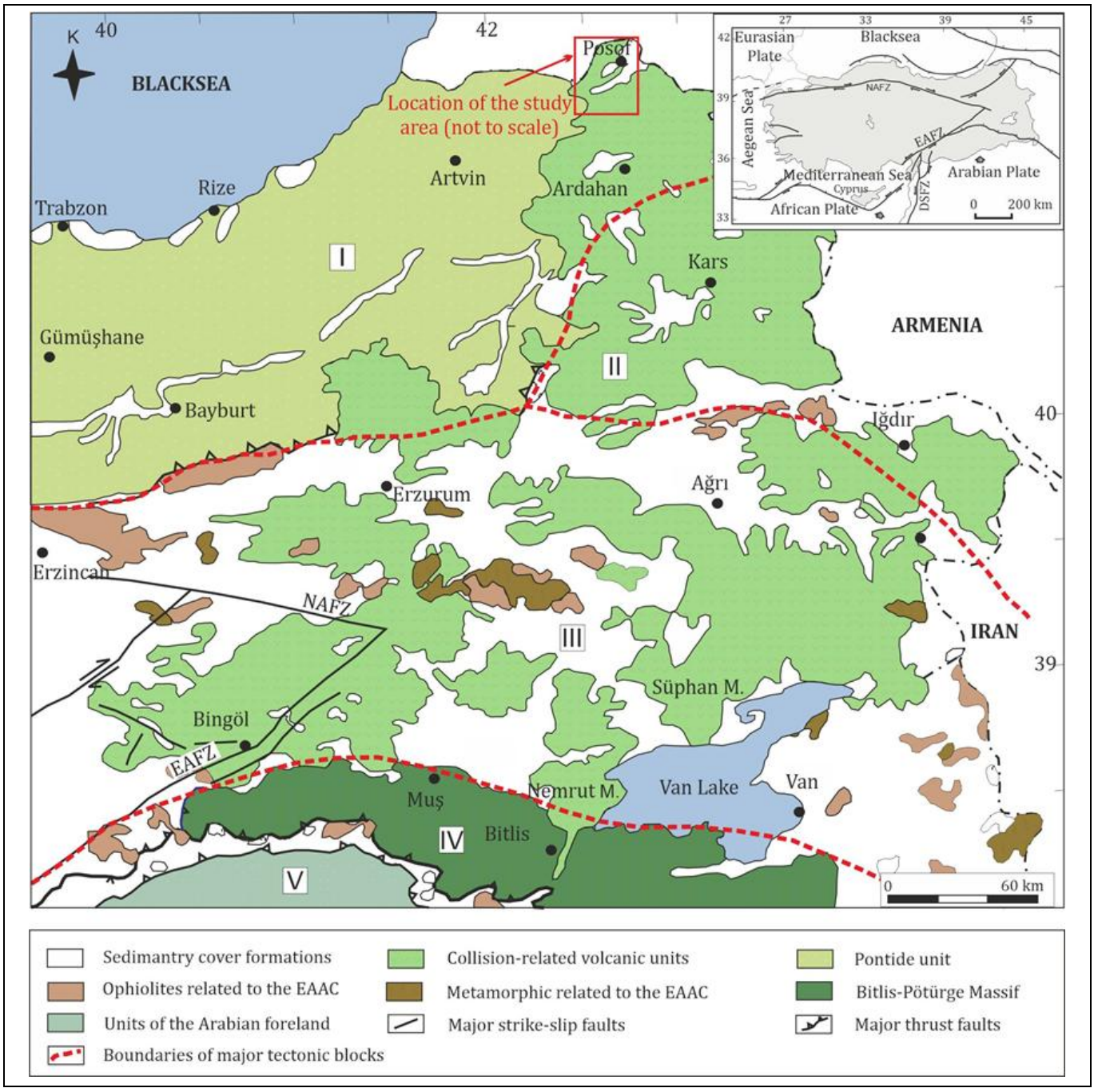

Figure 1. The inset map shows the tectonic units of Turkey and the distribution of collision-related volcanics in Eastern Anatolia. I: Rhodope-Pontide fragment, II: Northwest Iranian fragment, III: Eastern Anatolian Accretionary Complex (EAAC), IV: Bitlis-Pötürge Massif, V: Arabian Foreland. EAFZ: East Anatolian Fault Zone, NAFZ: North Anatolian Fault Zone (modified after [21]).

These five blocks are: (I) the Rhodope–Pontid unit which is including study area in the northeast, (II) the northwest-Iran section, (III) the Eastern Anatolian accretionary complex and the Anatolian basement, (IV) the Bitlis–Pötürge metamorphic massif, and (V) the Arabian foreland. These tectonic blocks are unconformably overlain by Oligocene–Middle Miocene sediments, which reflect a shallow marine environment in places. The Pontide basement rocks, which are represented by arc and post-collisional magmatic and the associated sedimentary rocks [22]-[33].

The basement rocks of the Eastern Pontides consist of Paleozoic metamorphic rocks [34],[35], metagranites [36] Late Carboniferous-aged granitic intrusions [37]-[40] and the Permo-Carboniferous sedimentary rocks [41]-[43]. These units have been crosscut by Late Triassic lamprophyres in the southern part of the Eastern Pontides [44]. The basement rocks are unconformably overlined by Early-Middle Jurassic volcanoclastic and sedimentary rocks [45]-[47]. All these units are cut by Early and Middle Jurassic intrusive rocks [48]- [52]. The Middle–Upper Jurassic–Cretaceous units composing of neritic and pelagic carbonates, conformably overlie Jurassic magmatic and volcano-clastic rocks [29],[53]. The Late Cretaceous series consists of sedimentary, volcanic rocks, their pyroclastics, and plutonic rocks [54]-[58]. Even if there are opposite reviews, the Eocene volcanism is ascribed to post-collisional [29],[59]. The Palaeocene to early Eocene magmatism is represented by adakitic or adakite-like volcanis [60]-[63]. The Late Cretaceous series and adakitic rocks are overlined by Eocene volcanic and volcaniclastic rocks [23],[24],[64]-[68]. The calc-alkaline granitoids of similar ages intruded into the Eocene volcanic and volcaniclastic rocks in the region [69]-[71]. The Miocene magmatism has limited propagation in the Eastern Pontides, and its affinity ranges from calc-alkaline to mildly and moderately alkaline [24], [31], [32], [72]. In the southern part of the Eastern Pontides, the Late Miocene are dacitic in composition, while Pliocene-Quaternary adakitic rocks are trachyandesite. The Late Miocene–Pleistocene volcanism generally extends to the North Anatolian Fault Zone (NAFZ) [73]-[78]. The Miocene volcanic rocks are overlain unconformably by the Miocene–Pliocene sedimentary rocks.

In the Eastern Anatolian block, the magmatic activity, which is ascribed to post-collisional, extends an area along ~ 500 km to the north of the Bitlis–Zagros suture (Figure 1). The Early Miocene granitoids and sub-volcanic intrusions are the first products in this block [79]-[81]. Intense collision-related volcanic activities started at the Middle Miocene (15 Ma) [79] and continue to the historical periods [82]-[86].

The southern branch of the Tethys Ocean, which began to close during the Late Cretaceous, separated the Anatolid–Tauride tectonic platform and the Eastern Anatolian Accretionary Complex (EAAC) from the African–Arabian plate, and the collision between the Arabian and Eurasian plates occurred along the Bitlis–Pötürge suture zone during the Middle Miocene [30]. The Eastern Anatolia region was formed under a north–south compressional regime that developed after the subduction of the northern branch of the Tethys Ocean and the subsequent continental collision between the Anatolian and Arabian plates since the Miocene [87]. As a result of this compressional regime, several tectonic structures such as strike-slip and thrust faults, and east–west–trending folds were formed [88]. Around 12–13 Ma, the collision between the Arabian and Eurasian plates caused the region to uplift by approximately 2 km above sea level [87]. This regional uplift led to the formation of volcanic sequences with distinct geochemical compositions across much of the area [89]. Volcanic activity, which is widespread throughout the region, mostly developed along extensional fissures [90]. Recent geophysical studies have revealed that crustal thickness varies from 38 km in the southern part of Eastern Anatolia to 50 km beneath the Erzurum–Kars Plateau in the north, with an average thickness of about 45 km [91]. These findings indicate a close relationship between the geodynamic evolution and volcanism of the region. The detachment and sinking of the subducted oceanic lithospheric slab into the asthenosphere [21],[92] led to a geochemical transition of magmatism from calc-alkaline to alkaline character[89],[92],[93]. The origin and evolution of magmatism in Eastern Anatolia remain subjects of ongoing debate. Various models have been proposed to explain the mantle source and lithospheric structure. Among them, partial lithospheric delamination (82) and slab break-off [21],[92] are the most widely accepted mechanisms. Recent studies have proposed refined versions of these models. Late Cenozoic magmatism has been associated with slab break-off and/or delamination related to the Arabia–Anatolia plate collision [94]. Volcanism began approximately 3.5 Ma with mildly alkaline basaltic lava flows, continued between 2.9 and 2.1 Ma with intermediate to acidic units (andesite–dacite), and concluded between 2.0 and 0.97 Ma with transitional and subalkaline basaltic lava flows [95]. In the Eastern Anatolian Collision Zone (EACZ), the shallowing of the lithosphere–asthenosphere boundary (LAB) from the Miocene to the Pliocene and the loss of the lithospheric mantle through delamination led to the formation of voluminous basaltic lavas during this period. In contrast, during the Quaternary, the deepening of the LAB and the thickening of the lithospheric mantle were associated with the re-accretion of the mantle lithosphere (relamination). It has been suggested that a lithospheric mantle layer 5–11 km thick could be re-accreted beneath the EACZ within approximately 5–6 Ma [96]. An alternative model suggests that volcanism in the region began in the Oligocene and was driven by lithospheric dripping processes triggered by intensified collision during the Late Miocene–Early Pliocene [97]. It has been suggested that volcanism, sedimentary basin development, uplift, and crustal deformation in the Eastern Anatolia region have evolved asymmetrically from north to South [98], and that this evolution is associated with a brittle lithospheric detachment process that has been ongoing for approximately 20 million years [99].

3 Material and method

Based on petrographic observations, the fresh and representative volcanic rock samples from the studied Late Miocene basic volcanic rocks were chosen to determine the mineral compositions of the samples. The major element composition of the clinopyroxene, olivine, feldspar, hornblende, brown mica, apatite, and Fe–Ti oxides were analysed by using a CAMECA SX100 instrument from the Laboratoire Magmas et Volcans (Clermont-Ferrand, France) with an accelerating voltage of 15 kV and sample current of 15 nA. Peak and background counting times ranged from 10s to 20s and 5s to 10s, respectively. Natural minerals and

synthetic/compounds were used as standards. Matrix effects were corrected by using Phi (r) z Peak Sight© software from CAMECATM. Typical standard deviations (1σ) ranged from 0.1 to 0.3 wt. % for Si, Ca, Na, and Al, and from 0.03 to 0.1 wt. % for Fe, Cr, K, Ti, Mg, and Mn.

4 Result

4.1.1 Local geology

The study area is situated around Posof and Damal vicinities (Ardahan, Turkiye) at the intersection of the Eastern Pontides and the north of the Eastern Anatolian region, including the Erzurum-Kars high plateau (Figure 1). The Posof volcanic roks generally displays grey, green and reddish brown, pale yellow, pinkish, and off-white colors, and their thickness varies from 90 to 300m [100]. This unit, which comprises the basement of the studied area, is unconformably covered by Posof volcanic rocks, which are composed of Late Miocene-aged basalt, tuff, and agglomerate, and sedimentary intercalations in it [100]. The Posof volcanic rocks, which are exhibited as light and pale grey, brown, and black colors, have wide propagations around the Posof vicinity, Cin Dağı, and Ulgar Tepe (Figure 2 and Figure 3). They are blocky and fractured, and generally have fine and coarse-grained plagioclase, pyroxene, and amphibole minerals in the hand specimen (Figure 3a, b, c, e, f). The large vesicles up to 15cm are observed in basalts, and most of them are unfilled, whereas some of them are filled with calcite (Figure 3d). The Pliocene-aged Ardahan andesite, which exhibits flow-texture, unconformably covers all the older units, while the Pleistocene-aged Ulgar Tepe andesite in phorphyritic texture is the youngest volcanic unit that crosscuts all the other older units in the study area. The Pleistocene detritic sediments, Holocene avalanches, and alluviums cover all these units (Figure 2).

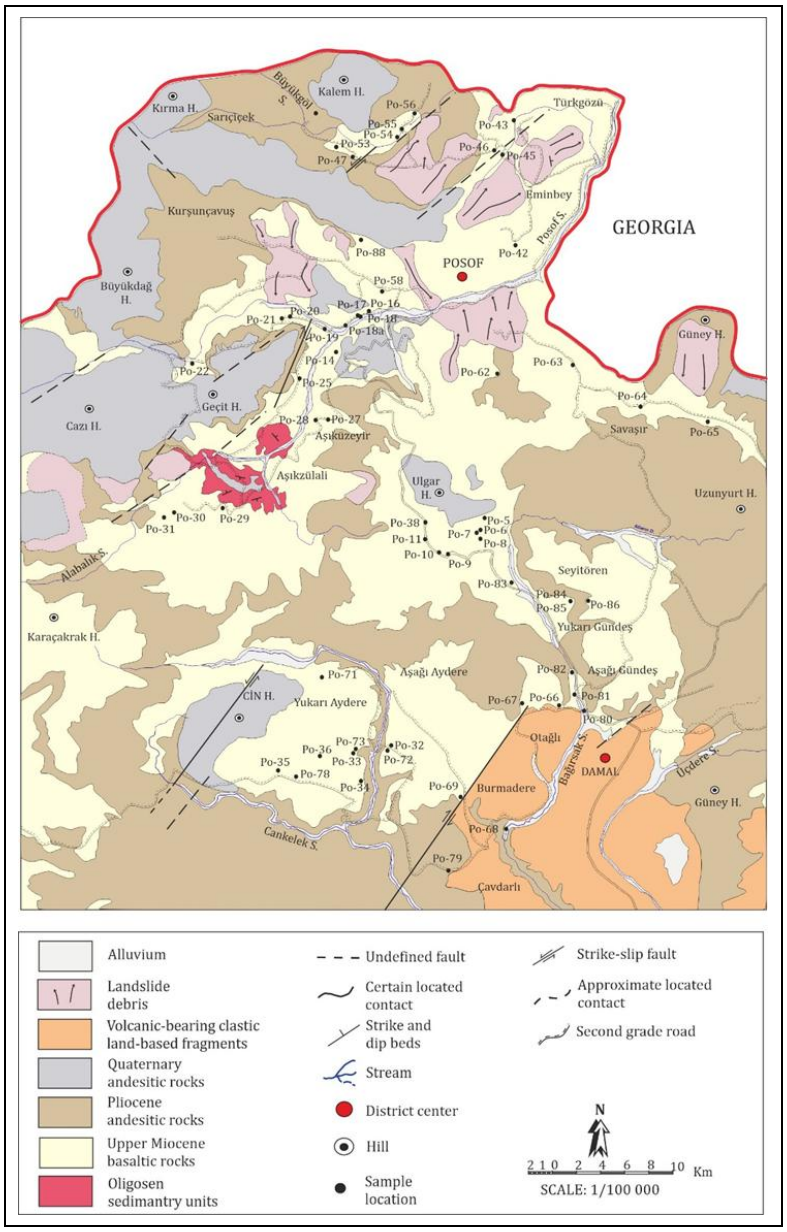

Figure 2. Geological map of the study area in 1/100 000 scale [Modified after [101].

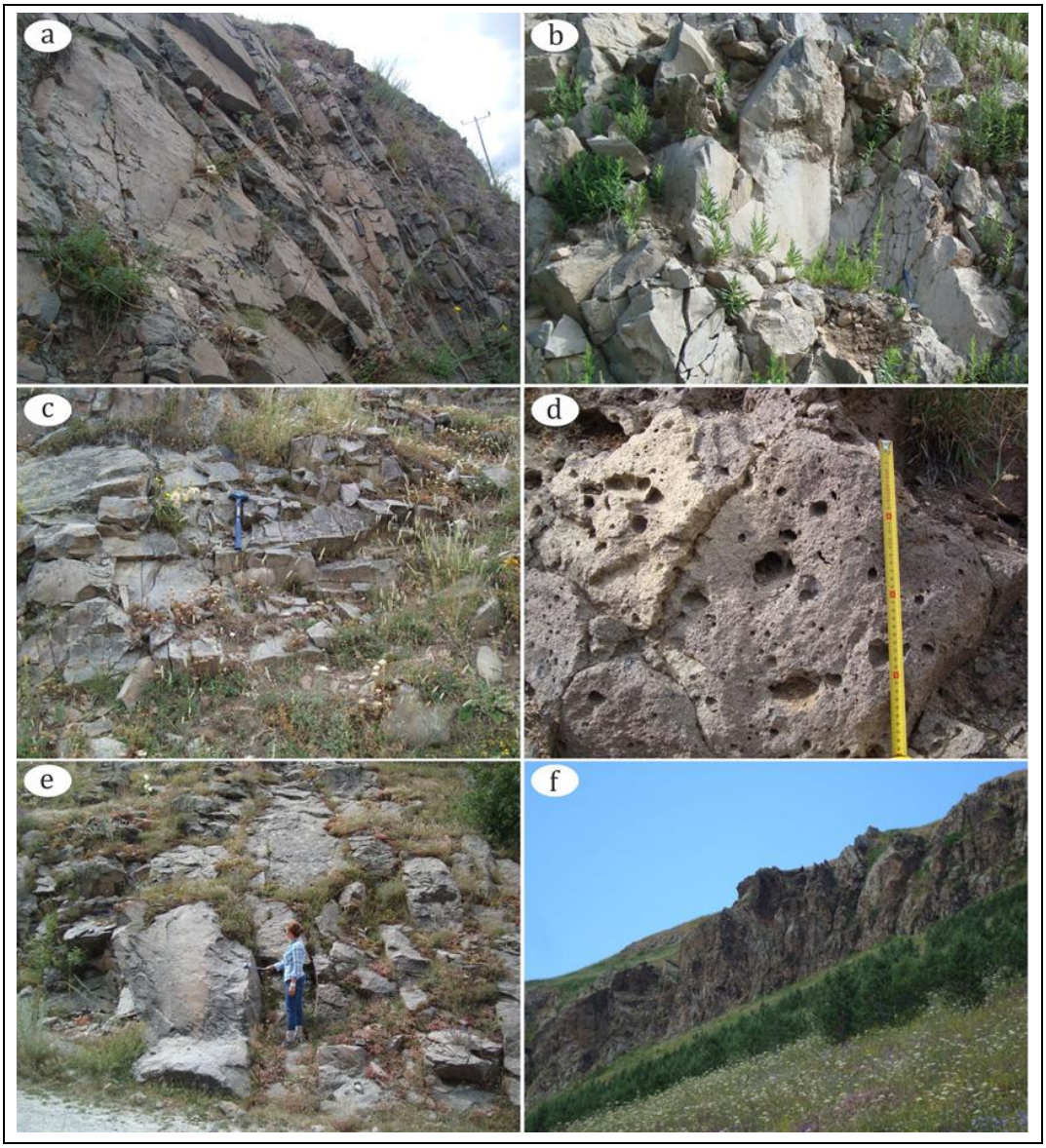

Figure 3. Macrophotograph of the Studied Late Miocene basic volcanic rocks. (a): The fractures observed in the studied volcanic rocks around the vicinity of Posof. (b): Altered volcanic rocks, light grey in colour. (c): Fractured basaltic rocks. (d): Vesicular basalts. (e): Blocky basalts around Kalem Tepe. (f): Appearance of the basaltic rocks in the study area.

4.2 Petrography

The Late Miocene volcanic rocks are generally microlithic, and some samples contain mega cysts rarely. The volcanic rocks, composition, consist of olivine, pyroxene, plagioclase, and opaque minerals in general, and they contain opacitized hornblende to a lesser extent. The groundmass of the volcanic rocks is generally composed of the microlites of the common minerals and the glass phase.

The microlithic porphyritic, hyalo-microlithic porphyritic textures are the most common in the studied volcanic rocks. The intergranular, pilotaxitic, subophitic, glomerophyric, fluidal, and vesicular textures are other textures observed in these volcanic rocks. Besides, the vesicles and the other cavities were filled with secondary minerals like calcite. The textural properties, which indicate disequilibrium crystallization, such as normal and reverse zoning, sieved texture, resorbed and embayed crystals, are present in all studied volcanic rocks. The dominant mineral phase composing the studied volcanic rocks is plagioclase. They are commonly euhedral, subhedral, magmas (Figure 4a, b, c). The resorbed and zoned crystals are the other evidence showing disequilibrium crystallization (Figure 4a). Pyroxenes are mostly euhedral and subhedral clinopyroxene, and orthopyroxene to a lesser extent. They appear as a phenocryst, microphenocrysts crysts and microlites in the groundmass, and some of them are fractured (Figure 4d, e). The pyroxenes also exhibit zoning, as in plagioclase, and include some mineral inclusions along their zones (Figure 4e). The olivines are euhedral, subhedral, and unhedral phenocrystals, and they were iddingsitized along their rims and fractures (Figure 4f). The opaque minerals are generally rounded and present in groundmass, pyroxenes, and plagioclases as inclusions (Figure 4e). The totally opacitized hornblendes are observed in some samples rarely.

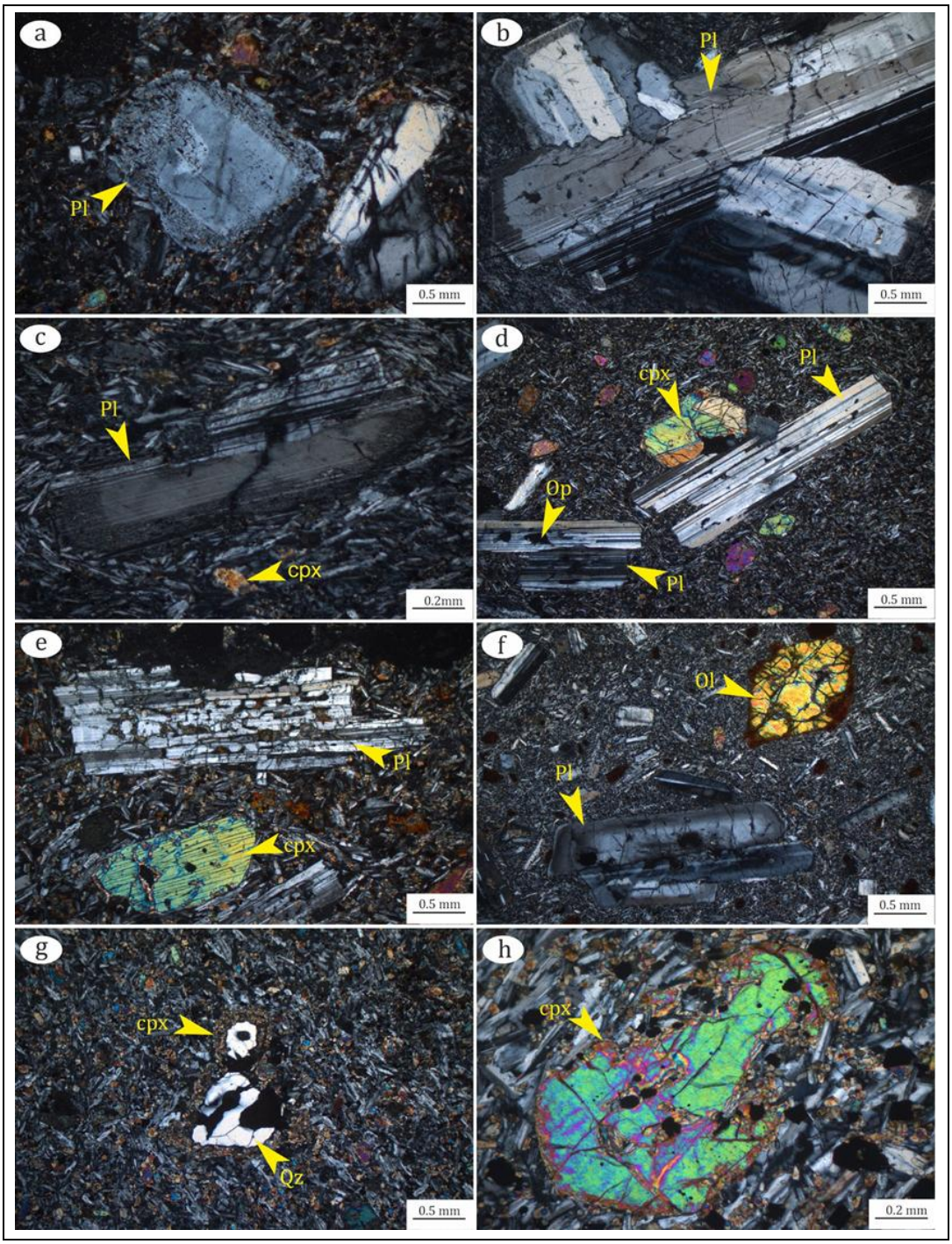

Figure 4. Microphotograph of; (a): Opaque inclusions bearing plagioclase and clinopyroxene phenocrysts in hyalomicolithic phorphyritic texture (Sample No: Po-18). (b): Euhedral olivine iddingsitized along rim and fractures and zoned plagioclase phenocrystal (Sample No: Po-36). (c): Sieved and resorbed rim of the plagioclase (Po-33). (d): Fractured plagioclase (Po-46, Ç.N.), (e, f): Sieved, resorbed and zoned plagioclase phenocryst (Po-65, Po-66), (g): reaction texture formed by micro-sized clinopyroxene crystals surrounding quartz xenocrysts (Po-38) (h): Bay-shaped clinopyroxene crystal (Po-31).

4.3 Mineral chemistry

The mineral chemistry analyses of olivine, pyroxene, plagioclase, hornblende, and opaque minerals situated in the Late Miocene volcanic rocks were performed on the core, mantle, and rim of the phenocrysts. Mineral chemistry analyses determined only the core composition of the microlites. Some phenocrysts, such as plagioclase and clinopyroxene, were analyzed to determine chemical variation through the profiles between core and rim. All mineral chemistry data are provided in the Appendix A-F.

4.3.1 Olivine

A large part of the olivine in Late Miocene volcanic rocks was situated in the magmatic olivine field in the diagram proposed by [102] while the others were determined to be mantle-originated olivine (Figure 5 and Appendix A). The CaO content of the magmatic olivines vary between 0.19 and 0.38, whereas the olivine of the mantle has CaO content between 0.15 and 0.19 wt.%. The olivine phenocrysts are classified as krizolite (Fo_{71-86}), and Hyalosiderite (Fo_{63-68}) according to their Fo contents. Only one analyzed olivine microlite is krizolite in composition with the Fo_{55} content.

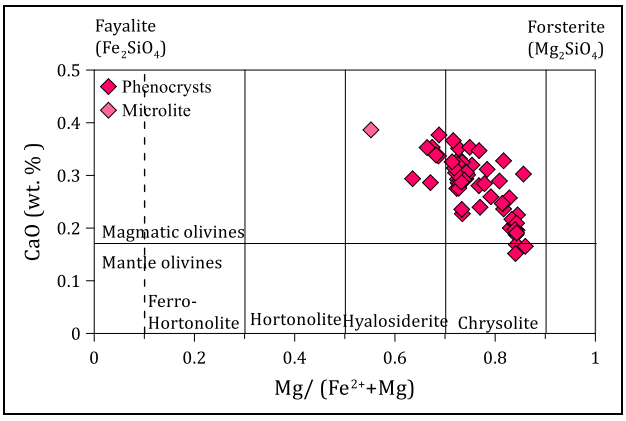

Figure 5. The Mg/(Fe^{2+}+Mg) versus CaO (wt.%) classification diagram of the olivines from Late Miocene basic volcanic rocks. The discrimination line is from [102].

4.3.2 Pyroxene

The pyroxenes were classified using the diagram of [103], and one part of them was identified as orthopyroxene in the clinoenstatite composition; the others were determined to be clinopyroxene in the augite composition (Figure 6 and Appendix B, C).

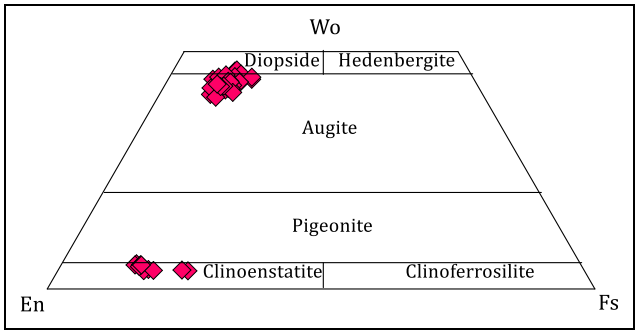

Figure 6. The Wo-Wn-Fs ternary classification diagram of the pyroxenes of the Late Miocene volcanic rocks [103].

The end-member compositions of clinoenstatite are $Wo_{3-4}En_{73-82}Fs_{14-24}$ with (Mg#) 0.75-0.86. These minerals are characterized by high MgO (26.53-30.74%), FeO (9.20-15.42%), and low Cr_2O_3 (0-0.20%), Al_2O_3 (1.10-3.67%), TiO_2 (0.05-0.27%) contents and are determined to be Fe-Mg clinoenstatite. Augites are $Wo_{39-45}En_{43-50}Fs_{11-12}$ in composition, with Mg# between 0.72-0.85, and characterized by high MgO (14.14-17.68%), FeO (5.31-9.56%), and low Cr_2O_3 (0-0.65%), Al_2O_3 (1.68–3.86%), TiO_2 (0.29-1.70%) contents. According to these chemical properties, they are determined to be Fe-Mg Augite. Both orthopyroxenes and clinopyroxenes display normal and reverse zoning with regard to their chemical variation between core and rim. The core Mg# of the normally zoned orthopyroxenes is 0.85, while rim compositions are 0.84. Reversely zoned orthopyroxenes have Mg# ranging from 0.75 to 0.85 in the core, 0.76 to 0.86 in the rim. The core compositions of the normally zoned clinopyroxene are in the range of 0.78-0.83, and the rim composition is in the range of 0.72-0.83, while the reversely zoned clinopyroxenes have Mg# in the range of 0.77-0.81 in core, and in the range of 0.80-0.84 in rim.

4.3.3 Plagioclase

The dominant mineral phase of the Late Miocene volcanic rocks is plagioclase, which is exhibited as phenocrysts and microlites in the groundmass (Figure 4b). The An content of the plagioclase phenocrysts and microlites observed in the studied volcanic varies between 16 and 77. They are Bytownite ($An_{72-77}Ab_{22-27}Or_1$), Labradorite ($An_{51-69}Ab_{30-48}Or_1$), and andesine ($An_{33-50}Ab_{48-64}Or_{2-3}$) in compositions. Most of the microlites are labradorite, and ($An_{52-66}Ab_{33-46}Or_{1-2}$) and andesine ($An_{16-48}Ab_{49-66}Or_{2-18}$) in compositions, except for a sample in anorthoclase composition (Figure 7 and Appendix D). Plagioclase phenocrystals generally display both normal and reverse zoning. Normally zoned plagioclases have a core composition of $An_{51-77}Ab_{22-48}Or_1$, and rim composition of $An_{34-63}Ab_{36-64}Or_{1-3}$, while the reversely zoned plagioclases have a core composition in the range of $An_{39-70}Ab_{30-59}Or_{0-2}$, and rim composition in the range of $An_{51-72}Ab_{27-46}Or_{1-3}$. Maximum anorthite variations between the core and the rim of normally zoned plagioclase are 29, and reversely zoned plagioclase are 12.

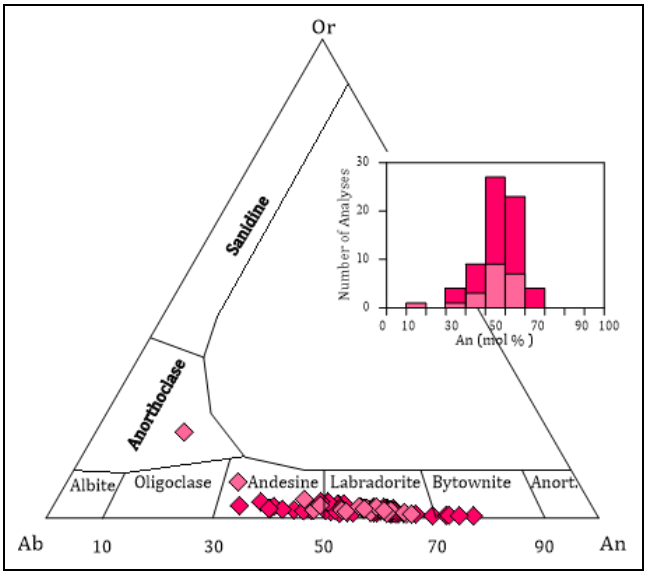

Figure 7. The Or-Ab-An ternary classification diagram of the plagioclases of the Late Miocene volcanic rocks.

4.3.4 Hornblende

The hornblendes of Late Miocene basic volcanic rocks are calcic in composition according to their chemical properties such as Si contents of 5.96-6.43, $Al^{[IV]}$ values of 1.80-2.27, Ti content of 0.21-0.38, $(Na+K)_A$ values of 0.95-1.27, $(Ca+Na)_B$ values of 1.98-2.00 and Mg# of 0.62-0.79 (Appendix E). The horblendes are classified as magnesio-hastingsite with $Al^{[VI]}<Fe^{3+}$ and pargasite with $Al^{[VI]}>Fe^{3+}$ according to the calcic amphibole classification of [104] (Figure 8).

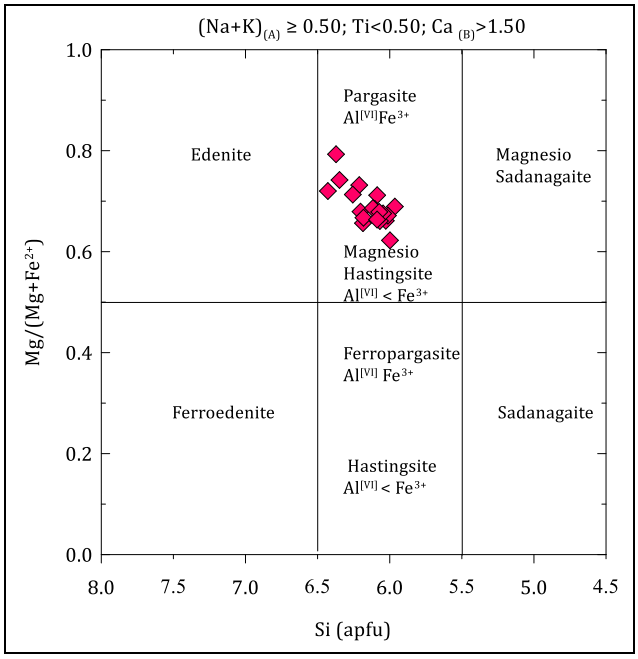

Figure 8. The Mg/(Mg+Fe^{2+}) versus Si (apfu) classification diagram of the hornblendes of the Late Miocene volcanic rocks [104].

4.3.5 Fe-Ti oxides

The opaque minerals in the studied volcanic rocks are generally present as rounded crystals and inclusions in other ferromagnesian minerals. They are mostly in magnetite and ulvospinel in compositions with $Usp_{0.05-1.44}$, except for three in ilmenite with $İlm_{0.94-0.96}$ compositions according to the classification of [105] (Figure 9 and Appendix F).

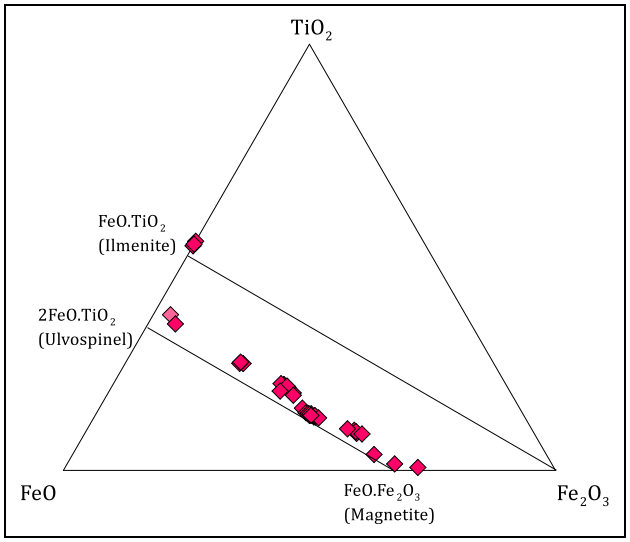

Figure 9. The classification diagram of the Fe-Ti oxides of the Late Miocene volcanic rocks [106].

4.3.6 Intensive parameters

The minerals and their equilibrium conditions with the melt, in which they reside, are controlled by physicochemical parameters such as temperature (T), pressure (P), and oxygen fugacity (fO_2).

Defining these parameters allows us to understand the crustal evolution and the crystallization history of the magmas that formed igneous rocks. Besides, the crystallization conditions of olmalıthe igneous rocks can be determined by investigation of the mineral paragenesis and composition with uncertainty as well. The crystallization temperature and pressure of the studied volcanic rocks based on mineral and melt compositions were determined by calibrations suggested by various researchers studying mineral thermodynamics. These calculations are generally practiced based on the equilibrium condition between mineral-mineral and mineral-melt.

4.3.7 Clinopyroxene thermobarometry

The equilibrium conditions between clinopyroxene and melt are the effective factor in estimating crystallization temperature, pressure, in connection with crystallization depth. This equilibrium condition, which is based on the temperature and pressure calculations, was investigated in detail by [20],[107]-[110]. An equilibrium constant was also determined based on Fe-Mg exchange and $K_D(Fe–Mg)^{cpx-liq}$ =0.27±0.03 by [20]. In case of the $K_D(Fe–Mg)^{cpx-liq}$ is in the desired range of 0.27±0.03, it is accepted that the mineral is in equilibrium with the melt. The composition of the groundmass glass or the bulk-rock composition of the rock can be used as a melt or liquid composition during thermobarometric calculations. The temperature and pressure estimates for the clinopyroxenes of the Late Miocene basic volcanic rocks obtained by using [20] calibrations and results are given in Table 1.

Table 1. Pressure and temperature estimates [20] derived from clinopyroxenes in the studied Late Miocene mafic volcanic rocks (n = number of analyses).

Clinopyroxene thermometry and barometry (n= 20)			
	P(kbar) Eqn 32b	T(°C) Eqn 32d	$K_D(Fe-Mg)^{cpx-liq}$ Eqn 35
Minimum	0.73	1026.50	0.27
Maximum	8.30	1230.30	0.29
Mean	4.16±2.02	1179.32±53.90	0.3

The crystallization temperatures were revealed to vary from 1026.50 °C to 1230.30°C (mean, 1179.32±53.90°C), and pressures yielded between 0.73 kbar and 8.30 kbar (mean, 4.16±2.02 kbar). The obtained crystallization pressures of the studied volcanic rocks indicate that the crystallization depth of the clinopyroxenes is between 2.76 km and 31.34 km ($P=\rho \cdot g \cdot z$, noting that 1 kbar=100 MPa and g=9.81 m/s^2, and to specify that you used a density value of 2.7 g/cm^3, which is reasonable for Eastern Anatolia (1 kbar=3.7 km for continental crust [111].

4.3.8 Hornblende thermobarometer, hygrometer, and oxygen fugacity

In the literature, there are several research studies to estimate crystallization pressure of the hornblendes in volcanic rocks. [11],[12], and [112] suggested calibrations that take into account $Al^{(T)}$ of hornblende and calculated the crystallization pressure. Apart from these, new thermobarometers are being developed nowadays[16],[17],[113]-[115]. [115] argued the new calibration, which is based on the major oxide content of the hornblende, and calculated the crystallization temperature, pressure, oxygen fugacity ($logfO_2$), and H_2O content of the magmas. The calculated crystallization temperatures and pressure of the hornblende in the studied volcanic rocks are

880.18°C to 1014.15°C (mean, 949±30.48°C), 2.53 kbar to 8.71 kbar (mean, 4.20±1.36 kbar), respectively (Table 2). The crystallization depth of the hornblendes was determined as 9.6-32.9 km (mean, 15.6 km) about the calculated crystallization pressures (1 kbar = 3.7 km for continental crust; [111].

Table 2. Temperature, pressure, hydrometer, and oxygen fugacity values derived from hornblendes in the studied Late Miocene volcanic rocks [115]; n = number of analyses).

Hornblende thermometry, barometry, hygrometry, and oxygen fugacity (n = 19)					
	T(°C)	P(kPa)	ΔNNO	logfO$_2$	(%)H$_2$O
Minimum	880.18	2.53	0.39	-10.94	4.60
Maximum	1014.15	8.71	1.76	-8.92	6.32
Mean	949.58± 30.48	4.20± 1.36	0.9± 0.42	-10.05± 0.48	5.34± 0.47

Oxygen fugacity (logfO$_2$) is a crucial parameter in crystallization processes of igneous rocks, and it can be identified as the partial pressure of oxygen during magma evolution. The thermodynamic condition, which is the function of temperature and pressure, and the stability boundaries of the rock-forming minerals are controlled by this parameter. There is a direct proportion between oxygen fugacity and temperature, and generally, an increase in temperature leads to an increase in oxygen fugacity [16], [116]. The oxygen fugacity values were obtained for hornblendes from the studied Late Miocene basic volcanic rocks that vary between -10.94 and -8.92 (mean, -10.05 ± 0.48). The relative oxygen fugacity (Nickel-Nickel Oxide, ΔNNO log units) range from 0.39 to 1.76 (mean, 0.92±0.42) (Table 2).

It is well known in literature that the H$_2$O content of the hornblende-bearing magmas is controversial. [117] suggest that this content is in the range of 2-3%, while it is an average 5% according to [118]-[120], and an average 6% according to [121]. The hornblendes in the studied volcanic rocks have H$_2$O content between 4.60 % and 6.32 % (mean, 5.34±0.47 %)(Table 2). The existence of the hornblende as a hydrous mineral shows that the magmas that formed the studied volcanic rocks have high H$_2$O and volatile content. [122] state that this type of high-temperature and water-content magmas can rise to shallow crustal levels without completely crystallizing.

The studied volcanic rocks were crystallized at a pressure between 2.5-9 kbar (250-900 PMa), and at a temperature between 900-1000 °C (Figure 10a). In the P-T diagram (Figure 10a), most of the hornblendes from Late Miocene basic volcanic rocks plot within domain of Tsc-Pgs±Pl±Ol±Cpx±Opx±Mgn±ilm and the other three samples plot in Tsc-Prg±Pl±Cpx±Opx±Mgn ± ilm domain, with nearly similar thermal stability values, such as 900°C to 1000°C. Furthermore, the hornblende from the studied volcanic rocks displays compatible behavior with the pink dashed curve, representing a 35% crystallinity curve. In the diagram of T(°C)-logfO$_2$ (Figure 10b), hornblendes plot between NNO and NNO+2 curves and are characterized by comparatively low oxygen fugacity values that vary from 10.94 to -8.92. The H$_2$O content of the samples is in the range of 4.60-6.32% and they plot between the stability field of consistent amphiboles, which is roughly constrained by the maximum stability curve and the (lower) limit of consistent amphibole crystallization in T(°C)-H$_2$Oerg diagram (Figure 10c).

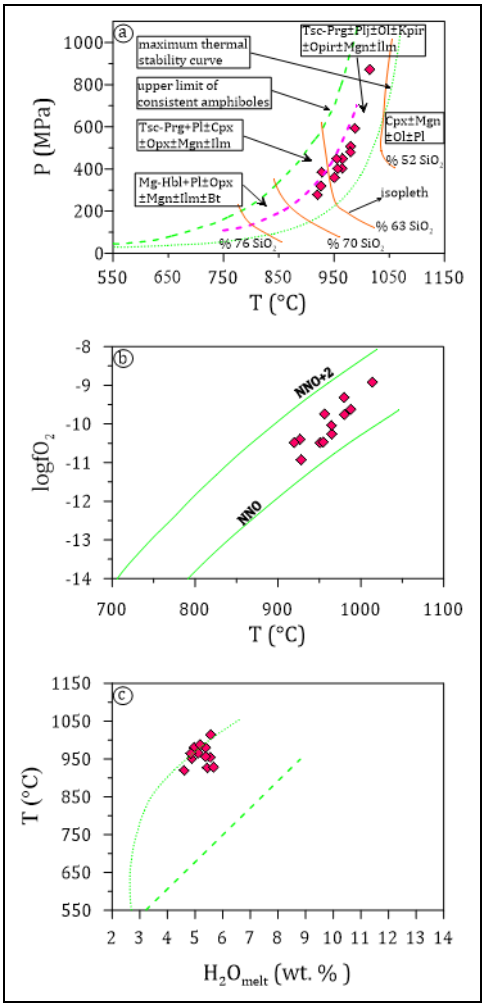

Figure 10. (a): P-T. (b): logfO$_2$-T ve (c): T-H$_2$O$_{liq}$ diagrams of hornblendes from the studied Late Miocene basic volcanic rocks [16].

5 Discussion

5.1 Disequilibrium parameters

It is well known that there is a close relation between the stability of minerals in the melt, where the minerals are present, and the chemical composition, volatile content, oxygen fugacity, pressure, and temperature. When the disequilibrated melt due to these parameters reaches the equilibrium conditions again, the zonation, dissolution, and resorption of the mineral shed light on determining and understanding the disequilibrium processes that the minerals experienced [123]-[132].

The existence of sieved plagioclase and both normal and sieved plagioclase in the same sample, observing resorbed, embayed plagioclases and pyroxenes [133],[134] are the petrographic evidence of disequilibrium crystallization. The sieved texture and resorptions (Figure 4a, b, c) observed along the rim of the plagioclase phenocrysts of the Late Miocene basic volcanic rocks indicate that the magmas that formed the studied volcanic rocks may have experienced magma mixing and/or assimilation processes during their crustal evolution [135]. [136] emphasize that the sieved texture in plagioclase can also be accepted as evidence for pressure release due to the rapid

ascent of the magma towards the surface. The sieved, resorbed, and embayed pyroxene crystals in the studied volcanic rocks are also evaluated as manifestations of magma mixing [3], [131],[137] and/or decompression [138] during the evolution of the magmas. Another disequilibrium texture is the reaction texture of the quartz (Figure 4g), which is formed by a quartz xenocryst surrounded by thin clinopyroxenes [139],[140]. The occurrence of ocelli quartz xenocrysts in the Posof volcanic basalts may serve as key evidence for magma chamber recharging (mixing) and reheating events associated with convection [141]. In basalts containing more than 51% SiO_2, quartz xenocrysts armored with granular clinopyroxene are commonly observed. Nevertheless, quartz xenocrysts are present even in the most mafic basalts [142].

5.2 The compositional variations observed in plagioclases

The normal zoning of plagioclase is generally explained by the single fractional crystallization phenomenon, while several hypotheses have been brought forward for the reverse zoning. They are:

(i) Pressure and temperature increase in water saturated conditions,

(ii) Temperature increase during ascent of the water saturated magma [143],

(iii) Back-mixing processes of crustal magma chambers [144] and

(iv) The temperature increase due to recharge of the magma chambers by the hotter magmas [131].

The anorthite (An) contents of the normally zoned plagioclases from Late Miocene volcanic rocks are in the range of An_{51-77} in the core, and in the An_{34-63} in the rim. Reversely zoned plagioclases characterized by an increase in An content from core to rim, have an An content of An_{39-70} in the core, and of An_{51-72} in the rim. The core and rim anorthite content of the plagioclases from the studied volcanic rocks shows variation in a wide interval (29% for normally zoned plagioclases, 12% for reversely zoned ones), and it is interpreted as crucial evidence for magma mixing processes [145].

The magma mixing and decompression cause disequilibrium, which is the reason for the genesis of textural and compositional changes. However, the burning question is which one is a more effective factor. Tracking the variation in TiO_2 content of plagioclases is a precious way to determine the reason for resorption, if it is related to magma mixing or pressure decrease [132]. The detailed mineral chemistry analyses of plagioclases from the studied volcanic rocks show that both normally and reversely zoned plagioclases are present in the same sample. It can be accepted as another evidence for magma mixing processes.

The TiO_2 content in the plagioclases from the studied volcanic rocks ranges from 0.00 to 0.21 wt.%. To track compositional changes between the core and the rim, ΔTiO_2 (TiO_{2core}-TiO_{2rim}) and $\Delta An(An_{core}–An_{rim})$ parameters were calculated. The negative trend in the ΔTiO_2 versus ΔAn (Figure 11b) diagram may result from TiO_2 increasing during magmatic differentiation or be explained by an increase in the partition coefficient as magma differentiates and An content decreases [146].

The negative correlation was observed in the An versus TiO_2 diagram of the core and the rim composition of the plagioclases from the studied volcanic rocks (Figure 11a). It is postulated that if the crystallization occurred in equilibrium conditions, the reason for the consistent negative trend is recharging the magma chamber by mafic magma that is leading high An, and low TiO_2 content, and/or contemporaneous fractional crystallization [146].

The normally zoned plagioclases from Late Miocene basic volcanic rocks display a magmatic differentiation (fractionations) trend with positive ΔAnR (1.18-29.30) and ΔTiO_2 values between -0.21 and 0.06 in the ΔAnR versus diagram, which shows resorption of plagioclases due to both pressure release and magma mixing.

The reversely zoned plagioclases display compatible variation with the primitive magma enrichment trend, with ΔTiO_2 varying from -0.05 to 0.08, and negative ΔAnR from -12.25 to -1.07 in Figure 11b. The crystallization of normally zoned plagioclase can be related to the recharging of the magma chamber by evolved magma, and this leads to negative ΔTiO_2 values, while reversely zoned plagioclases result from recharging to the magma chamber by hot and primitive magmas. Even if the plagioclases from the studied volcanic rocks are normally zoned, the reversely zoned plagioclases are also present in these volcanic rocks (Figure 11b). The presence of both resorbed and normal plagioclase crystals and normally and reversely zoned plagioclase in the same sample from the studied Late Miocene basic volcanic rocks can be explained by magma mixing during the evolution of the magmas.

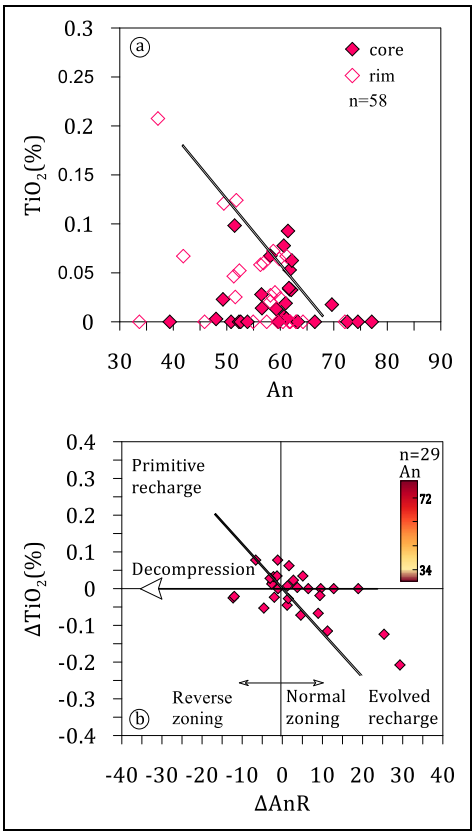

Figure 11. (a): An versus TiO_2 diagram showing the variations of core and rim of the plagioclases. (b): ΔAnR versus ΔTiO_2 diagram showing changes in normally and reversely zoned plagioclases of the Late Miocene basic volcanic rocks [146], (n: number of analyses).

5.3 The compositional variations observed in pyroxenes

The magmatic processes, such as magma mixing, recharging of magma chamber, fractional crystallization, and contamination, cause the textural and compositional properties of pyroxenes, and they play crucial role in interpreting these processes [147]-[160] argued five different hypotheses to put forward the purpose of the genesis of disequilibrium textures observed in clinopyroxenes:

(i) The mixing of the compositionally distinct magma bodies,

(ii) Fractional crystallization from the single magma body at low-pressure conditions,

(iii) The fractional crystallization at different pressures,

(iv) The presence of the xenocrystic cores indicating mantle origin or derivation from compositionally different source,

(v) Crystals represent early cumulates being crystallized from a parental magma to a zoned magma chamber and the back mixing of cumulates with evolved residual liquid. The clinopyroxes from the Late Miocene basic volcanic rocks display disequilibrium textures such as resorptions in the core and mantle of the crystals, and rounded crystals (Figure 4e, h). The generation of sieved texture, resorption, and erosion in clinopyroxenes can result from magma mixing [3],[131],[137] or decompression [138].

The normally zoned orthopyroxenes have Mg# in the range of 0.85 in the core and 0.84 in the rim. The Mg# of reversely zoned orthopyroxenes ranges from 0.75 to 0.85 in the cores and from 0.76 to 0.86 in the rims. (Figure 12a). The Mg# of the normally zoned clinopyroxenes varies between 0.78 and 0.83 in the core, and 0.72 and 0.83 in the rim. Reversely zoned clinopyroxenes are characterized by Mg# ranging from 0.77 to 0.81 in the core, and 0.80-0.84 in the rim (Figure 12b). In addition to these, the presence of the normally and reversely zoned orthopyroxenes and clinopyroxenes in a single sample may indicate magma mixing processes.

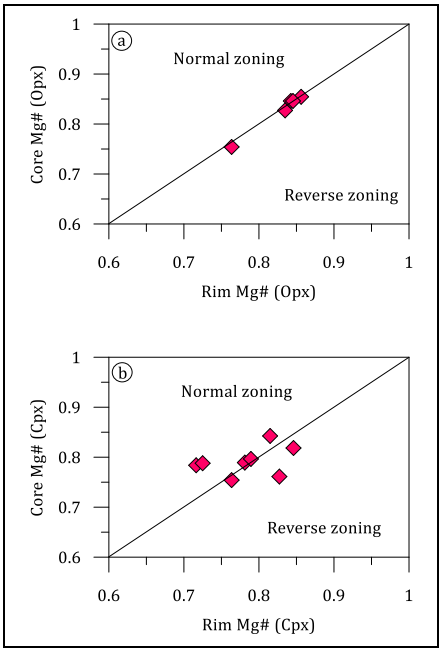

Figure 12. (a): Core-rim Mg number ((Mg/(Mg+Fe^{2+})) variations in orthopyroxes of the studied volcanics. (b): Core-rim Mg number ((Mg/(Mg+Fe^{2+})) variations in clinopyroxenes of the studied volcanics [162].

5.4 The crystallization history of the late miocene magmas

The study area, located at the intersection of the Eastern Pontides and the Erzurum-Kars Plateau, and its south, has been reported as having a crustal thickness of ~38 km in the south and ~50 km in the north, based on previous geophysical data [91],[161],[163], with an average thickness of 45 km [91].

Traces of magmatic processes at different depths (such as textural, petrographic, and chemical instabilities) are clearly observed in the studied Late Miocene volcanic rocks. Petrographic observations, mineral chemistry, and thermobarometric calculations indicate that magma evolution occurred in multiple magma chambers at different pressures and temperatures. Barometric data based on hornblende and clinopyroxene minerals were used to determine crystallization depth. According to these data, the magmatic system of the Late Miocene volcanism developed through magma chambers located at deep (20–30 km), middle (10–20 km), and shallow (0–10 km) levels. Maximum pressure values calculated from hornblende and clinopyroxene barometry correspond to the deep magma chamber at depths of 32 and 31 km, respectively.

Melting, assimilation, storage, and homogenization processes are effective in the hornblende and clinopyroxene phenocrysts that begin to crystallize at these levels [164]. At this level, hornblende crystallization occurred under moderate oxidation conditions, along with olivine and orthopyroxene with high forsterite (Fo) content. Hornblende and clinopyroxene crystallization occurred simultaneously in the magma, which continued to ascend and settled into the middle magma chamber at a depth of 15 km. Normal and reverse zoning, as well as rounded, sieve-like, and dissociated-edge crystal morphologies observed in the medium-anorthite-containing plagioclases, are clear indicators of magma mixing. The presence of normal and reverse-zoned plagioclases within the same sample indicates multiple magma intrusions within an open-system magma chamber. As magma ascended to depths between 2 and 9 km, its energy decreased, and the crystallization processes became more stable. Under high oxidation conditions, the crystallization of opacified hornblende crystals culminated in the formation of clinopyroxene at a depth of 2 km. At this level, melting and assimilation processes were limited, resulting in products closer to the final composition of the magma. In conclusion, the Late Miocene volcanic rocks studied reflect a multi-stage magmatic evolution that developed in magma chambers at different depths. When the petrographic, mineral chemistry, and geobarometric data are evaluated together, it is possible to conclude that the investigated volcanic rocks are derived from volatile-rich magmas under polybaric crystallization conditions.

6 Conclusions

The Late Miocene basic volcanic rocks consist of basalt, basaltic andesite, and andesite. Petrographic examinations indicate that these volcanic rocks commonly contain plagioclase, clinopyroxene, orthopyroxene, olivine, and opaque minerals (predominantly Fe-Ti oxides), while they locally include subordinate amounts of opaque hornblende. In these volcanic rocks, several textural features were identified, such as sieve texture, resorption texture, zoning, and the coexistence of both normally and reversely zoned plagioclases within the same sample. These features represent evidence for disequilibrium

crystallization. Mineral chemistry analyses reveal that the Late Miocene volcanic rocks are mainly composed of plagioclase (An_{16-77}), clinopyroxene ($Wo_{39-45}En_{43-50}Fs_{11-12}$), orthopyroxene ($Wo_{3-4}En_{73-82}Fs_{14-24}$), olivine ($Fo_{63-86}$), hornblende (Mg#0.62-0.79), and Fe-Ti oxides ($Usp_{0.05-1.44}$, $Ilm_{94.10-95.53}$). According to clinopyroxene-melt thermobarometry results indicate crystallization temperatures ranging from 1026.5 to 1230.3 °C (mean 1179.32 ± 53.9 °C) and crystallization pressures between 0.73 and 8.3 kbar (mean 4.16±2.02 kbar). Hornblende thermobarometry, hygrometry, and oxygen fugacity calculations yield crystallization temperatures between 880.18 and 1014.15 °C (mean 949±30.48°C), crystallization pressures between 2.53 and 8.71 kbar (mean 4.20±1.36 kbar), water contents ranging from 4.60 to 6.32 wt.% (mean 5.34±0.47 wt.%), and oxygen fugacity ($logfO_2$) values from (-10.94) to (-8.92) (mean -10.05±0.48). ΔNNO (Delta Nickel-Nickel Oxide) values range from 0.39 to 1.76 (mean 0.92±0.42). The occurrence of both normal and reverse zoning in clinopyroxenes and plagioclases reflects variable physicochemical conditions during magma evolution. Combined evaluation of the clinopyroxene and hornblende thermobarometry results suggests that the Late Miocene basic volcanic rocks crystallized from hydrous and volatile-rich basic magmas under oxidizing conditions at mid-to shallow-crustal levels, approximately 15 km depth, and at relatively high temperatures.

7 Acknowledgement

This research was financially supported by the Sci. Res. Projects Unit of Gümüşhane University, under project codes 22.F.5114.01.01. We thank the Ankara University, Earth Sciences Application and Research Center (YEBİM) for their collaboration in preparing the polished thin sections used for the mineral chemistry analyses. We acknowledge the collaboration of the Electron Microprobe Laboratory, Géosciences Marines (IFREMER), Université de Bretagne Occidentale (Brest, France), in performing the mineral chemistry analyses. We also thank editor and two anonymous reviewer for their constructive criticism and comments, which significantly improved the quality of this manuscript. This study builds upon a portion of the doctoral research by Cicerali (2025).

8 Author Contributions Statement

In the scope of this study; Derya Cicerali, fieldwork, literature review, acquisition of the map used, data collection, evaluation and interpretation of the results, and visualization; Cem Yücel, conceptualization, fieldwork, design, supervision, writing–review-editing, examination of the results, and overall quality and content control of the manuscript; Emre Aydınçakır, conceptualization, fieldwork and evaluation of the results; Abdullah Kaygusuz, design, evaluation of the results, 2nd supervision, and writing-review-editing were contributed at various stages of the study.

9 Ethics committee approval and conflict of interest statement

"There is no need to obtain permission from the ethics committee for the article prepared". "There is no conflict of interest with any person/institution in the article prepared".

10 References

[1] Dobosi G, Fodor FV. "Magma fractionation, replenishment, and mixing as inferred from green core clinopyroxenes in Pliocene basanite, Southern Slovakia". *Lithos,* 28, 133-150, 1992.

[2] Rutherford MJ, Hill PM. "Magma ascent rates from amphibole breakdown: an experimental study appliedtothe 1980-1986 Mount St. Helens eruptions". Journal of Geophysical Research, 98, 19667-19685, 1993.

[3] Simonetti A, Shore M, BelI K. "Diopside phenocrysts from Nephelinite lavas, Napak Volcano, Eastem Uganda: evidence for magma mixing". Canadian Mineralogist, 34, 411-421, 1996.

[4] Baxter S, Feely M. "Magma mixing and mingling textures in granitoids: examples from the Galway Granite, Connemara, Ireland". Mineralogy and Petrology, 76, 63-74, 2002.

[5] Kerr AC, Kent RW, Thomson BA, Seedhouse JK, Donaldson CH. "Geochemical evolution of the Tertiary Mull volcano, western Scotland". Journal of Petrology, 40, 873-908, 1999.

[6] Ma X, Meert JG, Xu Z, Zhao Z. "Evidence of magma mixing identified in the Early Eocene Caina pluton from the Gangdese Batholith, southern Tibet". Lithos, 278(281), 126-139, 2017.

[7] Michel L, Wenzel T, Markl G. "Interaction between two contrasting magmas in the Albtal pluton (Schwarzwald, SW Germany): textural and mineral-chemical evidence". International Journal of Earth Sciences, 5, 1505-1524, 2016.

[8] Weidendorfer D, Mattsson HB, Ulmer P. "Dynamics of magma mixing in partially crystallized magma chambers: textural and petrological constraints from the basal complex of the Austurhorn intrusion (SE Iceland)". Journal of Petrology, 55(9), 1865-1903, 2014.

[9] Abbott RN. "Muscovite-bearing granites in the AFM liquidus projection". Canadian Mineralogist, 23, 553-561, 1985.

[10] Speer JA. "Evolution of magmatic AFM mineral assemblages in granitoid rocks: the hornblende + melt = biotite reaction in the Liberty Hill pluton, South Carolina". American Mineralogist, 72, 863-878, 1987.

[11] Hollister LS, Grisson GC, Peters EK, Stowell HH, Sisson VB. "Confirmation of the empirical calibration of aluminum in amfibole with pressure of solidification of calc-alkaline plutons". American Mineralogist, 34, 243-256, 1987.

[12] Johnson MC, Rutherford MJ. "Experimental calibration of the aluminiun inhornblende geobarometer with application to Long Valley Caldera (California) volcanic rocks". Geology, 17, 837-841, 1989.

[13] Schmidt MW. "Amphibole composition in tonalite as a function of pressure: An experimental calibration of the Al-in-hornblende barometer". Contributions to Mineralogy and Petrology, 110, 304-310, 1992.

[14] Holland TJB, Blundy JD. "Non-ideal interactions in calcic amphiboles and their bearing on amphibole-plagioclase thermometry". Contribution to Mineralogy and Petrology, 116, 433-447, 1994.

[15] Anderson JL, Smith DR. "The effects of temperature and fO2 on the Al-inhornblende barometer". American Mineralogist, 80, 549-559, 1995.

[16] Ridolfi F, Renzulli A, Puerini M. "Stability and chemical equilibrium of amphibole in calc-alkaline magmas: An overview, new thermobarometric formulations and application to subduction-related volcanos". Contributions to Mineralogy and Petrology, 160, 45-66, 2010.

[17] Ridolfi F, Renzulli A. "Calcic amphiboles in calc-alkaline and alkaline magmas: thermobarometric and chemometric empirical equations valid up to 1130 °C and 2.2 Gpa". Contributions to Mineralogy and Petrology, 163, 877-895, 2012.

[18] Nimis P. "A clinopyroxene geobarometer for basaltic systems based on crystals structure modeling". Contributions to Mineralogy and Petrology, 121, 115-125, 1995.

[19] Nimis P, Taylor WR. "Single clinopyroxene thermobarometry for garnet peridotites. Part 1 Calibration andtesting of a Cr-in-cpx barometer and an enstatite-in-cpx thermometer". Contrib Mineral Petrol, 139, 541-554, 2000.

[20] Putirka KD. "Thermometers and barometers for volcanic systems". Reviews in Mineralogy and Geochemistry, 69, 61-120, 2008.

[21] Şengör AMC, Özeren S, Genç T, Zor E. "East Anatolian high plateau as a mantle-supported, North-south shortened domal structure". Geophysical Research Letters, 30(24), 8045, 2003.

[22] Aslan Z. "U-Pb zircon SHRIMP age, geochemical and petrographical characteristics of tuffs within calc-alkaline Eocene volcanics around Gümüşhane (NE Türkiye), Eastern Pontides". Neues Jahrbuch für Mineralogie, 187(3), 329-346, 2010.

[23] Arslan M, Temizel İ, Abdioğlu E, Kolaylı H, Yücel, C, Boztuğ D, Şen C. "40Ar–39Ar dating, whole-rock and Sr–Nd–Pb isotope geochemistry of post-collisional Eocene volcanic rocks in the southern part of the Eastern Pontides (NE Türkiye): implications for magma evolution in extension-induced origin". Contributions to Mineralogy and Petrology, 166(1), 113-142, 2013.

[24] Aslan Z, Arslan M, Temizel İ, Kaygusuz A. "K-Ar dating, whole-rock and Sr-Nd isotope geochemistry of calc-alkaline volcanic rocks around the Gümüşhane area: Implications for post-collisional volcanism in the Eastern Pontides, Northeast Türkiye". Mineralogy and Petrology, 108(2), 245-267, 2014.

[25] Aydınçakır E, Yücel C, Ruffet G, Gücer MA, Akaryalı E, Kaygusuz A. "Petrogenesis of post-collisional Middle Eocene volcanism in the Eastern Pontides (NE, Türkiye): Insights from geochemistry, whole-rock Sr-Nd-Pb isotopes, zircon U-Pb and 40Ar-39Ar geochronology". Geochemistry, 82, 2, 125871, 2022.

[26] Aydınçakır E, Yücel C, Kaygusuz A, Bilici Ö, Yilmazer S, Ruffet G. "Eocene magmatism related to postcollisional extension in the Eastern Pontides (NE Türkiye): 40Ar-39Ar geochronology, geochemistry, and whole-rock Sr-Nd-Pb-Hf isotopes". Turkish Journal of Earth Sciences, 33, 530–556, 2024.

[27] Kaygusuz A, Siebel W, Şen C, Satır M. "Petrochemistry and petrology of I-type granitoids in an arc setting: The composite Torul pluton, Eastern Pontides, NE Türkiye". International Journal of Earth Sciences, 97(4), 739–764, 2008,

[28] Kaygusuz A, Güloğlu ZS, Aydınçakır E, Yücel C, Vural A, Siebel W, Jeong Y-J. "U–Pb zircon dating, Sr-Nd whole-rock and Lu-Hf zircon isotope analyses of the Eocene Arslandede pluton, Eastern Pontides, NE Türkiye: Implications for mantle source and magma evolution". Geochemistry, 84, 126080, 2024.

[29] Okay Aİ, Şahintürk Ö. "Geology of the eastern Pontides. In: Robinson AG (Ed.) Regional and petroleum geology of the Black Sea and surrounding region". American Association of Petroleum Geologists (AAPG) Memoir, 68, 291–311, 1997.

[30] Şengör AMC, Yılmaz Y. "Tethyan evolution of Türkiye: a plate tectonic approach". Tectonophysics, 75, 181–241, 1981.

[31] Yücel C, Arslan M, Temizel İ, Abdioğlu Yazar E, Ruffet G. "Evolution of K-rich magmas derived from a net veined lithospheric mantle in an ongoing extensional setting: Geochronology and geochemistry of Eocene and Miocene volcanic rocks from Eastern Pontides (Türkiye)". Gondwana Research, 45, 65-86, 2017.

[32] Aydın F, Karslı O, Chen B. "Petrogenesis of the Neogene alkaline volcanics with implications for post-collisional lithospheric thinning of the Eastern Pontides, NE Türkiye". Lithos, 104(1–4), 249-266, 2008.

[33] Yücel C, Aydınçakır E, Kaygusuz A, Arslan M, Yi K, Jeong YJ, Cicerali D. "Petrogenesis of Late Cretaceous A-type plutonic rocks from the Eastern Pontides Orogenic Belt (NE Türkiye): constraints from zircon U-Pb geochronology, zircon Lu-Hf and whole-rock Sr-Nd-Pb-Hf isotopes". International Geology Review, 66(11), 2055–2078, 2024.

[34] Topuz G, Altherr R, Kalt A, Satir M, Werner O, Schwarz WH. "Aluminous granulites from the Pulur complex, NE Türkiye: A case of partial melting, efficient melt extraction and crystallisation". Lithos, 72(3–4), 183–207, 2004.

[35] Dokuz A, Gücer MA, Karslı O, Yi K. "From Cadomian back-arc basin to Rheic Ocean closure: the geochronological records of the Kurtoğlu Massif, eastern Sakarya Zone, Türkiye". International Journal of Earth Sciences, 111, 1333-1355, 2022.

[36] Karsli O, Şengün F, Dokuz A, Kandemir R, Aydin F. "Silurian to early Devonian arc magmatism in the western Sakarya Zone (NW Türkiye) with inference to the closure of the Rheic Ocean". Lithos, 370–371, 105641, 2020(a).

[37] Topuz G, Altherr R, Siebel W, Schwarz WH, Zack T, Hasözbek A, Barth M, Satır M, Şen C. "Carboniferous high-potassium I-type granitoid magmatism in the Eastern Pontides: The Gümüşhane pluton (NE Türkiye)". Lithos, 116(1–2), 92–110, 2010.

[38] Dokuz A. "A slab detachment and delamination model for the generation of Carboniferous high-potassium I-type magmatism in the Eastern Pontides, NE Türkiye: The Köse composite pluton". Gondwana Research, 19(4), 926–944, 2011.

[39] Kaygusuz A, Arslan M, Siebel W, Sipahi F, Ilbeyli N. "Geochronological evidence and tectonic significance of Carboniferous magmatism in the southwest Trabzon area, eastern Pontides, Türkiye". International Geology Review, 54(15), 1776–1800, 2012.

[40] Kaygusuz A, Arslan M, Sipahi F, Temizel İ. "U–Pb zircon chronology and petrogenesis of Carboniferous plutons in the northern part of the Eastern Pontides, NE Türkiye: Constraints for Paleozoic magmatism and geodynamic evolution". Gondwana Research, 39, 327–346, 2016.

[41] Çapkınoğlu Ş. "First records of conodonts from the permo-Carboniferous of demirözü (Bayburt), eastern Pontides, NE Türkiye", Turkish Journal of Earth Sciences 12, 199-217, 2003.

[42] Topuz G, Altherr R, Schwarz WH, Dokuz A, Meyer HP. "Variscan amphibolite-facies rocks from the Kurtoğlu metamorphic complex (Gümüşhane area, Eastern Pontides, Türkiye)". International Journal of Earth Sciences, 96(5), 861–873, 2007.

[43] Kandemir R, Lerosey-Aubril R. "First report of a trilobite in the Carboniferous of eastern Pontides, NE Türkiye". Turkish Journal of Earth Sciences, 20, 179–183, 2011.

[44] Karsli O, A. Dokuz A, Kaliwoda M, Uysal I, Aydin F, Kandemir R, Fehr KT, Wijbrans RJ. "Geochemical fingerprints of Late triassic calc-alkaline lam prophyres from the eastern Pontides, NE Türkiye: A key to understanding lamprophyre formation in a subduction-related environment". Lithos, 196–197, 181–197, 2014.

[45] Kandemir R, Yılmaz C. "Lithostratigraphy, facies, and deposition environment of the Lower Jurassic Ammonitico Rosso type sediments (ARTS) in the Gümüşhane area, NE Türkiye: Implications for the opening of the northern branch of the Neo-Tethys Ocean". Journal of Asian Earth Sciences, 34, 586–598, 2009.

[46] Saydam Eker Ç, Arı UV. "Geochemistry of the Middle Jurassic sediments in Gümüşhane, north-eastern Türkiye: Implications for weathering and provenance". Geological Journal, 55(7), 4954–4976, 2020.

[47] Saydam Eker Ç, Sipahi F, Kaygusuz A. "Trace and rare earth elements as indicators of provenance and depositional environments of Lias cherts in Gumushane, NE Türkiye". Geochemistry, 72(2), 167–177, 2012.

[48] Eyuboğlu Y, F.O. Dudas, M. Santosh, Xiao Y, Yi K, Chatterjee N, Wu FY, Bektaş O. "Where are the remnants of a Jurassic ocean in the eastern Mediterranean region?", Gondwana Research, 33, 63-91, 2016.

[49] Karslı O, Dokuz A, Kandemir R. "Zircon Lu-Hf isotope systematics and U–Pb geochronology, whole-rock Sr-Nd isotopes and geochemistry of the early Jurassic Gokcedere pluton, Sakarya Zone-NE Türkiye: a magmatic response to roll-back of the Paleo-Tethyan oceanic lithosphere". Contributions to Mineralogy and Petrology, 172(5), 31, 2017.

[50] Dokuz A, Aydınçakır E, Kandemir R, Karsli O, Siebel W, Derman AS, Turan M. "Late Jurassic magmatism and stratigraphy in the Eastern Sakarya zone, Türkiye: Evidence for the slab breakoff of paleotethyan oceanic lithosphere". Journal of Geology, 125, 1–31, 2017.

[51] Aydınçakır E, Gündüz R, Yücel C. "Emplacement conditions of magma(s) forming Jurassic plutonic rocks in Gümüşhane (Eastern Pontides, Türkiye)". Bulletin of the Mineral Research and Exploration, 162, 175–196, 2020.

[52] Aydınçakır E, Yücel C, Kaygusuz A, Bilici Ö, Yi K, Jeong YJ, Güloğlu ZS. "Magmatic evolution of the Calc-alkaline Middle Jurassic igneous rocks in the eastern pontides, NE Türkiye: insights from geochemistry, whole-rock Sr-Nd-Pb, in situ zircon Lu-Hf isotopes, and U-Pb geochronology". International Geology Review, 65,1–22, 2023.

[53] Saydam Eker Ç, Korkmaz S. "Mineralogy and whole rock geochemistry of late Cretaceous sandstones from the eastern Pontides (NE Türkiye)". Neues Jahrbuch fur Mineralogie, Abhandlungen, 188(3), 235–256, 2011.

[54] Çamur MZ, Güven İH, Er M. "Geochemical characteristics of the eastern Pontide volcanics: an example of multiple volcanics cycles in arc evolution". Turkish Journal of Earth Sciences, 5, 2, 123–144, 1996.

[55] Arslan M, Tüysüz N, Korkmaz S, Kurt H. "Geochemistry and petrogenesis of the eastern Pontide volcanic rocks, Northeast Türkiye". Chemie der Erde, 57, 157–187, 1997.

[56] Aydınçakır E. "Subduction-related Late Cretaceous high-K volcanism in the Central Pontides orogenic belt: constraints on geodynamic implications". Geodinamica Acta, 28(4), 379–411, 2016.

[57] Kaygusuz A, Siebel W, Ilbeyli N, Arslan M, Satir M, Şen C. "Insight into magma genesis at convergent plate margins a case study from the eastern Pontides (NE Türkiye)". Neues Jahrbuch fur Mineralogie Abhandlungen, 187(3), 265–287, 2010.

[58] Kaygusuz A, Arslan M, Temizel İ, Yücel C, Aydınçakır E. "U–Pb zircon ages and petrogenesis of the Late Cretaceous I-type granitoids in arc setting, Eastern Pontides, NE Türkiye". Journal of African Earth Sciences, 174, 104040, 2021.

[59] Boztuğ D, Jonckheere R, Wagner GA, Yeğingil Z. "Slow Senonian and fast Palaeocene-Early Eocene uplift of the granitoids in the Central Eastern Pontides, Türkiye: Apatite fission-track results". Tectonophysics, 382(3–4), 213–228, 2004.

[60] Topuz G, Altherr R, Schwarz WH, Siebel W, Satır M, Dokuz A. "Post-collisional plutonism with adakite-like signatures: The Eocene Saraycik granodiorite (Eastern Pontides, Türkiye)". Contributions to Mineralogy and Petrology, 150(4), 441–455, 2005.

[61] Karslı O, Dokuz A, Uysal I, Aydın F, Kandemir R, Wijbrans J. "Generation of the Early Cenozoic adakitic volcanism by partial melting of mafic lower crust, Eastern Türkiye: Implications for crustal thickening to delamination". Lithos, 114(1–2), 109–120, 2010.

[62] Dokuz A, Uysal I, Siebel W, Turan M, Duncan R, Akçay M. "Post-collisional adakitic volcanism in the eastern part of the Sakarya Zone, Türkiye: Evidence for slab and crustal melting". Contributions to Mineralogy and Petrology, 166(5), 1443–1468, 2013.

[63] Eyuboğlu Y, Santosh M, Chung SL."Crystal fractionation of adakitic magmas in the crust-mantle transition zone: Petrology, geochemistry and U-Pb zircon chronology of the Seme adakites, eastern Pontides, NE Türkiye". Lithos, 121(1–4), 151–166, 2011.

[64] Arslan M, Aliyazicioğlu I. "Geochemical and petrological characteristics of the kale (gümüshane) volcanic rocks: Implications for the eocene evolution of eastern pontide arc volcanism, Northeast Türkiye". International Geology Review, 43(7), 595–610, 2001.

[65] Aydınçakır E. "The petrogenesis of Early Eocene non-adakitic volcanism in NE Türkiye: Constraints on the geodynamic implications". Lithos, 208, 361–377, 2014.

[66] Kaygusuz A, Arslan M, Siebel W, Şen C. "Geochemical and Sr-Nd isotopic characteristics of post-collisional calc-alkaline volcanics in the eastern pontides (NE Türkiye)". Turkish Journal of Earth Sciences, 20(1), 137–159, 2011.

[67] Temizel İ, Arslan M, Yücel C, Abdioğlu E, Ruffet G. "Geochronology and geochemistry of Eocene-aged volcanic rocks around the Bafra (Samsun, N Türkiye) area: Constraints for the interaction of lithospheric mantle and crustal melts". Lithos, 258–259, 92–114. 2016.

[68] Kaygusuz A, Yücel C, Aydınçakır E, Gücer MA, Ruffet G. "40Ar–39Ar dating, whole-rock and Sr-Nd isotope geochemistry of the Middle Eocene calc-alkaline volcanic rocks in the Bayburt area, Eastern Pontides (NE Türkiye): Implications for magma evolution in an extension-related setting". Mineralogy and Petrology, 116(5), 379–399, 2022.

[69] Arslan M, Aslan Z. "Mineralogy, petrography and whole-rock geochemistry of the Tertiary granitic intrusions in the Eastern Pontides, Türkiye". Journal of Asian Earth Sciences, 27(2), 177-193, 2006.

[70] Kaygusuz A, Yücel C, Arslan M, Sipahi F, Temizel İ, Çakmak G, Güloğlu ZS. "Petrography, mineral chemistry and crystallization conditions of Cenozoic plutonic rocks located to the north of Bayburt (Eastern Pontides, Türkiye)". Bulletin of the Mineral Research and Exploration, 157, 75–102, 2018.

[71] Kaygusuz A, Güloğlu ZS, Aydınçakır E, Yücel C, Vural A, Saydam Eker Ç, Cicerali D. "Zircon U-Pb geochronology and Sr-Nd-Pb-Hf-O isotope signatures of Middle Eocene high-K plutons from the Eastern Pontides Orogenic Belt, NE Türkiye: implications for parental magma sources and magmatic processes". International Geology Review, 67(10), 1322–1352, 2025.

[72] Yücel C, Arslan M, Temizel İ, Abdioğlu E. "Volcanic facies and mineral chemistry of Tertiary volcanics in the northern part of the Eastern Pontides, northeast Türkiye: Implications for pre-eruptive crystallization conditions and magma chamber processes". Mineralogy and Petrology, 108(3), 439–467, 2014.

[73] Terlemez I, Yılmaz A. "Ünye-Ordu-KoyulhisarReşadiye arasında kalan yörenin stratigrafisi", Türkiye Jeoloji Kurultay Bulteni, 23(2), 179–191, 1980.

[74] Terzioğlu MN. "Reşadiye-Aybastı-Gölköy-Mesudiye ve Koyulhisar arasında yayılım gösteren Tersiyer Kuvaterner yaşlı volkanitlerin litostratigrafik özellikleri". Yerbilimleri: Cumhuriyet Üniversitesi, Mühendislik Fakültesi Dergisi, 29, 119–132, 1986.

[75] Ekici T. "Petrology and Ar/Ar choronology of Erdembaba and kuyucak volcanics exposed along the North Anatolian fault zone (eastern Pontides, NE Türkiye): Implications for the late cenozoic geodynamic evolution of eastern mediterra nean region". Journal Geology Society of India, 87(4), 411–423, 2016.

[76] Adiyaman Ö, Chorowicz J, Arnaud O, Gündogdu M, Gourgaud A. "Late Cenozoic tectonics and volcanism along the north anatolian fault: New structural and geo chemical data". Tectonophysics, 338(2), 135–165, 2001.

[77] Tatar O, Yurtmen S, Temiz H, Gürsoy H, Koçbulut F, Mesci BL, Guezou JC. "Intracontinental quaternary volcanism in the Niksar PullApart Basin, North Anatolian Fault Zone, Türkiye". Turkish Journal of Earth Sciences, 16(4), 391-412, 2007.

[78] Karslı O, Chen B, Uysal I, Aydın F, Wijbrans JR, Kandemir R. "Elemental and Sr–Nd–Pb isotopic geochemistry of the most recent Quaternary volcanism in the Erzincan Basin, Eastern Türkiye: framework for the evaluation of basalt–lower crust interaction". Lithos, 106(1–2), 55–70, 2008.

[79] Lebedev VA, Volkov VN, Sagatelyan AK, Chernyshev AIV. "Spatial migration of magmatic activity within the Caucasian segment of the alpine belt in the early Neogene under the conditions of geotectonic setting change: isotope geochronological data". Doklady Earth Sciences, 448, 225–231, 2013.

[80] Topuz G, Candan O, Zack T, Chen F, Li QL. "Origin and significance of Early Miocene high-potassium I-type granite plutonism in the East Anatolian plateau (the Taşlıçay intrusion)". Lithos, 348-349, 105210, 2019.

[81] Oyan V. "Ar-Ar dating and petrogenesis of the Early Miocene Taşkapı-Mecitli (Erciş-Van) granitoid, Eastern Anatolia Collisional Zone, Türkiye". Journal of Asian Earth Sciences, 158, 210–226, 2018.

[82] Pearce JA, Bender JF, De Long SE, Kidd WSF, Low PJ, Güner Y, Saroğlu F, Yılmaz Y, Moorbath S, Mitchell JG. "Genesis of collision volcanism in eastern Anatolia Türkiye". J Volcanol Geoth Res, 44, 189–229, 1990.

[83] Özdemir Y, Güleç N. "Geological and Geochemical evolution of Suphan Stratovolcano Eastern Anatolia, Türkiye: evidence for the lithosphere-asthenosphere interaction on post collisional volcanism". Journal of Petrology, 55, 37–62, 2014.

[84] Oyan V, Keskin M, Lebedev VA, Chugaev AV, Sharkov EV. "Magmatic Evolution of the Early Pliocene Etrüsk Stratovolcano, Eastern Anatolian Collision Zone, Türkiye". Lithos, 256(257), 88–108, 2016.

[85] Kaygusuz A. "K/Ar ages and geochemistry of the post-collisional volcanic rocks in the Ilıca (Erzurum) area, eastern Türkiye". Neues Jahrbuch fur Mineralogie Abhandlungen, 186(1), 21–36, 2009.

[86] Kaygusuz A, Aslan Z, Aydınçakır E, Yücel C, Gücer MA, Şen C. "Geochemical and Sr-Nd-Pb isotope characteristics of the Miocene to Pliocene volcanic rocks from the Kandilli (Erzurum) area, Eastern Anatolia (Türkiye): Implications for magma evolution in extension-related origin". Lithos, 296–299, 332–351, 2018.

[87] Şengör AMC, Kidd WSF. "Post-collisional tectonics of the Turkish–Iranian plateau and a comparison with Tibet". Tectonophyssics, 55, 361–376, 1979.

[88] Yılmaz Y, Şaroglu F, Güner Y. "Initiation of the neo magmatismin East Anatolia". Tectonophysics, 137, 177–199, 1987.
[89] Keskin M. "Eastern Anatolia: A hotspot in a collision zone without a mantle plume". Special Paper of the Geological Society of America, 430, 693–722, 2007.
[90] Keskin M, Pearce JA, Mitchell JG. "Volcano-stratigraphy and geochemistry of collision-related volcanism on the Erzurum-Kars Plateau Northeastern Türkiye". Journal of Volcanology and Geothermal Research, 85, 355-404, 1998.
[91] Zor E, Sandvol E, Gürbüz C, Türkelli N, Seber D, Barazangi M. "The crustal structure of the East Anatolian plateau (Türkiye) from receiver functions". Geophysical Research Letters, 30(24), 8044, 2003.
[92] Keskin M. "Magma generation by slab steepening and breakoff beneath a subduction-accretion complex: An alternative model for collision-related volcanism in Eastern Anatolia, Türkiye". Geophysical Research Letters, 30, 1-4, 2003.
[93] Oyan V. "Etrüsk Volkanı ve Çevresinin (Van Gölü kuzeyi) Volkanostratigrafisi Petrolojisi ve Magmatik Evrimi". Doktora Tezi, Yüzüncü Yıl Üniversitesi Fen Bilimleri Enstitüsü Van, 2011.
[94] Özdemir Y, Oyan V, Jourdan F. "Petrogenesis of Middle Miocene to Early Quaternary basalts from the Karayazı–Göksu plateau (Eastern Anatolia, Türkiye): Implication for the role of pyroxenite and lithospheric thickness". Lithos, 416–417, 106671, 2022.
[95] Özdemir Y, Özdemir A. "Deciphering the magma storage conditions and preeruptive processes at Cumaçay: a Plio-Quaternary volcanic eruption center in Eastern Anatolia, Türkiye", Turkish Journal of Earth Sciences, 32(2), 181–199, 2023.
[96] Oyan V, Özdemir Y, Chugaev AV,·Oyan E, Chernyshev IV. "Petrogenesis of Miocene to Quaternary primitive basaltic magmas in the area of Lake Van (East Anatolia, Türkiye): a case for relamination of mantle lithosphere after lithospheric delamination". Contributions to Mineralogy and Petrology, 178, 88, 2023.
[97] Oyan E, Oyan V, Özdemir Y, Güleç N. "Origin and petrogenesis of magmatism in collision-related environments: evidence from the Melikler Volcanics on the Kars Plateau- Türkiye in the Turkish-Iranian High Plateau". Journal of Petrology, 64, 1–26, 2023.
[98] Memiş C, Göğüş OH, Uluocak EŞ, Pysklywec R, Keskin M, Şengör AC, Topuz G. "Long wavelength progressive plateau uplift in Eastern Anatolia since 20 Ma: Implications for the role of slab peel-back and break-off". Geochemistry, Geophysics, Geosystems, 21(2), 1-24, 2020.
[99] Aktağ A, Sayit K, Furman T, Peters BJ. "Delamination Magmatism in Eastern Anatolia: A Geochemical Perspective". Geochemistry, Geophysics, Geosystems, 25(5), 1-18, 2024.
[100] Karaköse C, Asutay HJ, Yergök AF, Akbaş B, Dalkılıç H, Mengi H, Kara H, Papak İ, Keskin İ. "Ardahan-Posof Dolayının Jeolojisi". Jeoloji Etütleri Dairesi, Maden Tetkik ve Arama Genel Müdürlüğü, Ankara, Türkiye, Rapor No:492, 1994.
[101] Keskin İ. "Türkiye Jeoloji Haritaları Ardahan E49-F49 Paftaları". Maden Tetkik ve Arama Genel Müdürlüğü, Ankara, Türkiye, 181, 16, 2013.
[102] Thompson RN, Gibson SA. "Transient high temperatures in mantle plume heads inferred from magnesian olivines in Phanerozoic picrites". Nature, 407, 502-506, 2000.
[103] Morimoto M, Fabries J, Ferguson AK, Ginzburg IV, Ross M, Seifert FA, Zussman J, Aoki K, Gottardi G. "Nomenclature of pyroxenes". Mineralogical Magazine, 52, 535-550, 1988.
[104] Leake BE, Woolley AR, Arps CES. "Nomenclature of amphiboles: report of the subcomittee on amphiboles of the international mineralogical association, commission on new minerals and mineral names". Am Mineral, 82, 1019-1037, 1997.
[105] Lindsley DH, Spencer KJ. "Fe-Ti oxide geothermemetry: Reducing analyses of coexisting Ti-magnetite (Mt) and ilmenite (Ilm)" transactions". American Geophysical Union, 63, 471, 1982.
[106] Bacon CR, Hirschmann MM. "Mg/Mn partitioning as a test for equilibrium between coexiting Fe-Ti oxides". American Mineralogist, 73, 57-61, 1988.
[107] Putirka KD, Johnson M, Kinzler R, Walker D. "Thermobarometry of mafic igneous rocks based on clinopyroxene-liquid equilibria, 0-30 kbar". Contributions to Mineralogy and Petrology, 123, 92-108, 1996.
[108] Putirka K. "Clinopyroxene+liquid equilibrium to 100 kbar and 2450 K". Contributions to Mineralogy and Petrology, 135, 151-163, 1999.
[109] Putirka KD, Ryerson FJ, Mikaelian H. "New igneous thermobarometers for mafic and evolved lava compositions, based on clinopyroxene+liquid equilibria". American Mineralogist, 88, 1542-1554, 2003.
[110] Putirka KD. "Igneous thermometers and barometers based on plagioclase+liquid equilibria: Tests of some existing models and new calibrations". American Mineralogist, 90, 336-346, 2005.
[111] Tulloch AJ, Challis GA. "Emplacement depths of Paleozoic-Mesozoic plutons from western New Zealand estimated by hornblende-Al geobarometry". New Zealand Journal of Geology and Geophysics, 43, 555-567, 2000.
[112] Hammarstrom JM, Zen E. "Aluminum in hornblende: An empirical igneous geobarometer". American Mineralogist, 71, 1297-1313, 1986.
[113] Mutch EJF, Blundy JD,· Tattitch BC, Cooper FJ, Brooker RA. "An experimental study of amphibole stability in low-pressure granitic magmas and a revised Al-in-hornblende geobarometer". Contrib Mineral Petrol, 171, 85, 2016.
[114] Putirka K. "Amphibole thermometers and barometers for igneous systems and some implications for eruption mechanisms of felsic magmas at arc volcanoes". American Mineralogist, 101(4), 841-858, 2016.
[115] Ridolfi F. "Amp-TB2: An updated model for calcic amphibole thermobarometry". Minerals, 11(3), 324, 2021.
[116] Wones DR. "Significance of the assemblage titanite+magnetite+quartz in granitic rocks". American Mineralogist, 74, 744-749, 1989.

[117] Luhr JF, Carmichael ISE, Varekamp JC. "The 1982 eruptions of El Chicón Volcano, Chiapas, Mexico: Mineralogy and petrology of the anhydrite-bearing pumices". Journal of Volcanology and Geothermal Research, 23, 69-108, 1984.
[118] Eggler DH. "Water-saturated and undersaturated melting relations in a Paricutin andesite and an estimate of water content in the natural magma". Contributions to Mineralogy and Petrology, 34, 261-271, 1972.
[119] Helz RT. "Phase relations of basalts in their melting ranges at PH2O=5 kb as a function of oxygen fugacity". Journal of Petrology, 14, 249-302, 1973.
[120] Naney RT. "MT. "Phase equilibria of rock-forming ferromagnesian silicates in granitic systems". American Journal of Science, 283, 993-1033,1983.
[121] Merzbacher C, Eggler DH. "A magmatic geohygrometer: application to Mount St. Helens and other dacitic magmas". Geology, 12, 587-590, 1984.
[122] Helmy HM, Ahmed AF, El Mahallawi MM, Ali SM. "Pressure, temperature and oxygen fugacity conditions of calc-alkaline granitoids, Eastern Desert of Egypt and tectonic implications". Journal of African Earth Sciences, 38, 255-268, 2004.
[123] Grove TL, Baker MB, Kinzler RJ. "Coupled CaAl-NaSi diffusion in plagioclase feldspar: experiments and applications to cooling rate speedometry". Geochim Cosmochim Acta, 48, 2113-2121, 1984.
[124] Chakraborty S. "Diffusion in solid silicates: a tool to track timescales of processes comes of age". Annual Review of Earth and Planetary Sciences, 36, 153-190, 2008.
[125] Dohmen R, Faak K, Blundy JD. "Chronometry and speedometry of magmatic processes using chemical diffusion in olivine, plagioclase and pyroxenes". Reviews in Mineralogy and Geo chemistry, 83(1), 535-575, 2017.
[126] Cooper KM. "Time scales and temperatures of crystal storage in magma reservoirs: implications for magma reservoir Dynamics". Philosophical Transactions of the Royal Society, 377(2139), 2019.
[127] Costa F, Shea T, Ubide T. "Diffusion chronometry and the timescales of magmatic processes". Nature Reviews Earth and Environment, 1(4), 201-214, 2020.
[128] Petrone CM, Mangler MF. "Elemental diffusion chronostratigraphy. Crustal magmatic system evolution: Anatomy Architecture, and Physico-Chemical Processes". 177-193, 2021.
[129] Ginibre C, Wörner G. "Variable parent magmas and recharge regimes of the Parinacota magma system (N. Chile) revealed by Fe, Mg and Sr zoning in plagioclase". Lithos, 98, 18-140, 2007.
[130] Rutherford MJ, Devine JD. Magmatic conditions and processes in the storage zone of the 2004-2006 Mount St. Helens dacite. In: Sherrod DR, Scott WE, Stauffer PH Eds. A Volcano Rekindled: The first year of renewed eruption at Mount St. Helens, 2004-2006, United States Geological Survey Professional Paper, 703-726, 2008.
[131] Streck MJ. "Mineral textures and zoning as evidence for open system processes. in: Putirka KD, Tepley III FJ (eds). Minerals, inclusions and volcanic processes". Mineralogical Society of America and Geochemical Society, Review Mineral, 69, 1, 595-622, 2008.
[132] Bennett EN, Lissenberg, CJ, Cashman KV. "The significance of plagioclase textures in mid ocean ridge basalt (Gakkel Ridge, Arctic Ocean)". Contributions to Mineralogy and Petrology, 174, 49, 2019.
[133] Stimac JA, Pearce TH. "Textural evidence of mafic-felsic magma interaction in dacite lavas, Clear Lake, California". American Mineralogist, 77, 795-809, 1992.
[134] Venezky DY, Rutherford MJ. "Preeruption conditions and timing of dacite andesite magma mixing in the 2.2 Ka eruption at mount Rainier". Journal of Geophysical Research, 102, 20069-20086, 1997.
[135] Tsuchiyama A. "Dissolution kinetics of plagioclase in the melt system diopside albite-anorthite, and origin of dusty plagioclase in andesites". Contrib Mineral Petrol, 89, 1-16, 1985.
[136] Pearce TH, Russel JK, Wolfson I. "Laser-interference and normarski ınterference ımaging of zoning profiles in plagioclase phenocrysts from the May 18, 1980 eruption of Mount St. Helens, Washington". American Mineralogist, 72, 1131-1143, 1987.
[137] Hibbard MJ. "The magma mixing origin of mantled feldspars". Contributions to Mineralogy and Petrology, 76, 158-170, 1981.
[138] Nelson ST, Montana A. "Sieve-textured plagioclase in volcanic rocks produced by rapid decompression". Am Mineral, 77, 1242-1249, 1992.
[139] Shelley D. "Igneous and metamorphic rocks under the microscobe". Chapman and Hall, London, 445, 1993.
[140] Vernon HR. "A Practical Guide to Rock Microstructure". Cambridge University Press, 594, 2004.
[141] Jankovics MÉ, Sági T, Astbury RL, Petrelli M, Kiss B, Ubide T, Németh K, Ntaflos T, Harangi S. "Olivine major and trace element compositions coupled with spinel chemistry to unravel the magmatic systems feeding monogenetic basaltic volcanoes". Journal of Volcanolgy and Geothermal Research, 369, 203–223, 2019.
[142] Novak SW, Bacon CR. "Pliocene Volcanic Rocks of the Coso Range, Inyo County, California". U.S. Geologıcal Survey Professıonal Paper 1383, Unıted States Government Prıntıng Office, Washington, 1383, 49, 1986.
[143] Blundy J, Cashman K, Humhreys M. "Magma heating by decompression-driven crystallization beneath andesite volcanoes". Nature, 443, 76-80, 2006.
[144] Couch S, Sparks RSJ, Carroll MR. "Mineral disequilibriumin lavas explained by convective self-mixing in open magma chambers". Nature, 411, 1037-1039, 2001.
[145] Wallace PJ, Carmichael ISE. "Petrology of volcan tequila, jalisco, Mexico: disequilibrium phenocryst assemblages and evolution of the subvolcanic magma system". Contributions to Mineralogy and Petrology, 117, 345-361, 1994.
[146] Bedard JH. "Partitioning coefficients between olivine and sili cate melts". Lithos, 83, 394-419, 2005.
[147] Batki A, Pál-Molnár E, Dobosi G, Skelton A. "Petrogenetic significance of ocellar camptonite dykes in the Ditrău Alkaline Massif, Romania". Lithos, 200-201, 181-196, 2014.
[148] Codarcea A, Codarcea DM, Ianovici V. "Structura geologică a masivului de roci alkaline de la Ditrău. Buletin Ştiinţific", Secţia de Geologie şi GeografieII, (3-4), 385-446, 1957.

[149] Fall A, Bodnar RJ, Szabó Cs, Pál-Molnár E. "Fluid evolution in the nepheline sye nites of the Ditrău Alkaline Massif, Transylvania, Romania". Lithos, 95, 331-345, 2007.
[150] Kräutner HG, Bindea G. "Timing of the Ditrău alkaline intrusive complex (Eastern Carpathians, Romania)". Slovak Geological Magazine, 4, 213-221, 1998.
[151] Morogan V, Upton BGJ, Fitton JG. "The petrology of the Ditrău alkaline complex, Eastern Carpathians". Mineralogy and Petrology, 69, 227-265, 2000.
[152] Pál-Molnár E. Hornblendites and Diorites of the DitrăuSyeniteMassif. Ed. Department of Mineralogy, Geochemistry and Petrology. University of Szeged, Szeged, 172 2000.
[153] Pál-Molnár E. Rock-forming minerals of the Ditrău Alkaline Massif. In: Szakáll, S., Kristály, F. (Eds.), Mineralogy of Székelyland, Eastern Transylvania, Romania". Ed. Csík County Nature and Conservations Society, Sfântu Gheorghe-Miercurea-Ciuc-Târgu Mureș, 63-88, 2010(b).
[154] Pál-Molnár E, Batki A, Almási E, Kiss B, Upton BGJ, Markl G, Odling N. "Origin of mafic and ultramafic cumulates from the Ditrău Alkaline Massif, Romania". Lithos, 239, 1-18, 2015(b).
[155] Pál-Molnár E, Árva-Sós E. "K/Ar radiometric dating on rocks from the northern part of the Ditrău Syenite Massif and its petrogenetic implications". Acta Mineralogica- Pertrographica, 36, 101-116, 1995.
[156] Streckeisen A. "Das Nephelinsyenit-Massiv von Ditro (Siebenbürgen)". II. Teil. Schweizeriche Mineralogische und Petrographische Mitteilungen, 34, 336-409, 1954.
[157] Streckeisen A. "On the structure and origin of the nepheline-syenite complex of Ditro (Transylvania, Romania)". Report of the 21th International Geological Congress, 13, 228-238, 1960.
[158] Streckeisen A, Hunziker JC. "On the origin of the Nephelinsyenit Massif of Ditró (Transylvania, Romania)". Schweizerische Mineralogische und Petrographische Mitteilungen, 54, 59-77, 1974.
[159] Perugini D, Poli G, Christofides G, Eleftheriadis G. "Magma mixing in the sithonia plutonic complex, Greece: evidence from mafic microgranular enclaves". Mineralogy and Petrology, 78, 173-200, 2003.
[160] Dallmeyer DR, Kräutner HG, Neubauer F. "Middle-late Triassic 40Ar/39Ar hornblende ages for early intrusions within the Ditrău Alkaline Massif, Rumania: implications for Alpine rifting in the Carpathian orogen". Geologica Carpathica, 48, 347-352, 1997.
[161] Al- Lazki AI, Seber D, Sandvol E, Türkelli N, Mohamad R, Barazangi M. "Tomographic Pn velocity and anisotropy structure beneath the Anatolian plateau (Eastern Türkiye) and the surrounding regions". Geophysical Research Letters, 30, 24, 8043, 2003.
[162] Yücel C., "Trabzon-Giresun Arasındaki Tersiyer Volkanitlerinin Petrografisi, 40Ar-39Ar Jeokronolojisi, Petrokimyası, Sr-Nd-Pb İzotop Jeokimyası ve Petrolojisi", Doktora Tezi, Karadeniz Teknik Üniversitesi, Fen Bilimleri Enstitüsü, 285 sayfa, 2013.
[163] Sandvol E, Türkelli, N, Barazangi M. "The Eastern Türkiye Seismic Experiment: The study of a young continent-continent collision". Geophysical Research Letters, 30, 24, 8038, 2003.
[164] Hildreth W, Moorbath S. "Crustal contributions to arc magmatism in the Andes of central Chile". Contrib Mineral Petrol, 98, 455-489, 1988.

Appendix A.

Electron microprobe analysis results of olivine phenocrysts from Late Miocene basic volcanic rocks.

Sample	Po-17	Po-17	Po-17	Po-17	Po-17	Po-17	Po-17	Po-17	Po-17	Po-17	Po-17	Po-17	Po-17	Po-21	Po-21	Po-21	Po-21	Po-21
Mineral	c4	c4	c4	c4	c5	c7	c7	c8	c8	c9	c9	c9	c9	c1	c1	c2	c2	c2
	ol1	ol1	ol2	ol2	ol	ol1	ol1	ol1	ol1	ol1	ol1	ol2	ol3	ol1	ol1	ol1	ol1	ol2
	pheno	pheno	pheno	pheno	pheno	pheno	pheno	pheno	pheno	pheno	pheno	pheno	pheno	pheno	pheno	pheno	pheno	pheno
	core	rim	core	rim	core	core	rim	core	rim	core	rim	core	core	core	rim	core	rim	core
SiO_2	40.07	39.54	39.84	39.60	39.74	39.95	40.02	39.68	40.13	40.27	40.12	39.46	37.05	38.74	37.68	37.38	36.67	37.45
TiO_2	0.00	0.00	0.03	0.00	0.00	0.00	0.00	0.00	0.00	0.00	0.00	0.00	0.06	0.00	0.00	0.00	0.00	0.01
Al_2O_3	0.06	0.02	0.06	0.05	0.07	0.04	0.04	0.02	0.06	0.04	0.01	0.03	0.22	0.04	0.08	0.02	0.00	0.03
Cr_2O_3	0.00	0.00	0.01	0.00	0.00	0.00	0.00	0.00	0.00	0.01	0.00	0.02	0.00	0.00	0.00	0.00	0.00	0.00
FeO	14.99	15.87	14.84	15.07	14.65	14.71	15.62	14.88	15.07	13.33	15.03	14.75	15.01	20.11	25.80	28.89	31.90	27.91
MnO	0.26	0.39	0.29	0.31	0.33	0.33	0.35	0.28	0.30	0.21	0.40	0.33	0.35	0.35	0.43	0.46	0.55	0.45
MgO	44.72	43.52	44.48	44.13	44.69	44.45	43.82	44.71	44.20	46.02	44.46	44.31	50.18	40.93	36.56	33.56	31.18	34.53
NiO	0.31	0.14	0.29	0.20	0.25	0.38	0.19	0.33	0.35	0.49	0.22	0.21	0.25	0.13	0.10	0.05	0.00	0.09
CaO	0.19	0.20	0.17	0.21	0.23	0.20	0.22	0.21	0.20	0.17	0.15	0.19	0.30	0.31	0.37	0.35	0.29	0.38
Total	100.70	99.73	100.18	99.57	100.01	100.08	100.31	100.14	100.39	100.58	100.40	99.46	103.56	100.61	101.05	100.72	100.63	100.88
Si	1.00	1.00	1.00	1.00	1.00	1.00	1.01	1.00	1.01	1.01	1.01	0.99	0.93	0.99	0.99	1.00	1.00	0.99
Ti	0.00	0.00	0.00	0.00	0.00	0.00	0.00	0.00	0.00	0.00	0.00	0.00	0.00	0.00	0.00	0.00	0.00	0.00
Al	0.00	0.00	0.00	0.00	0.00	0.00	0.00	0.00	0.00	0.00	0.00	0.00	0.01	0.00	0.00	0.00	0.00	0.00
Cr	0.00	0.00	0.00	0.00	0.00	0.00	0.00	0.00	0.00	0.00	0.00	0.00	0.00	0.00	0.00	0.00	0.00	0.00
Fe^{2+}	0.31	0.34	0.31	0.32	0.31	0.31	0.33	0.31	0.32	0.28	0.32	0.31	0.32	0.43	0.57	0.65	0.72	0.62
Mn	0.01	0.01	0.01	0.01	0.01	0.01	0.01	0.01	0.01	0.00	0.01	0.01	0.01	0.01	0.01	0.01	0.01	0.01
Mg	1.67	1.64	1.67	1.66	1.67	1.66	1.64	1.67	1.66	1.72	1.66	1.66	1.88	1.56	1.43	1.34	1.26	1.37
Ni	0.01	0.00	0.01	0.00	0.01	0.01	0.00	0.01	0.01	0.01	0.00	0.00	0.00	0.00	0.00	0.00	0.00	0.00
Ca	0.01	0.01	0.00	0.01	0.01	0.01	0.01	0.01	0.01	0.00	0.00	0.01	0.01	0.01	0.01	0.01	0.01	0.01
Total	3.00	3.00	3.00	3.00	3.00	3.00	2.99	3.00	3.00	3.04	3.01	2.98	3.15	3.01	3.01	3.00	3.00	3.00
Mg#	0.84	0.83	0.84	0.84	0.84	0.84	0.83	0.84	0.84	0.86	0.84	0.84	0.86	0.78	0.72	0.67	0.64	0.69
Fo	83.94	82.67	83.97	83.64	84.17	84.05	83.03	84.02	83.68	85.84	83.71	83.96	85.34	78.10	71.30	67.08	63.13	68.45
Fa	15.78	16.91	15.72	16.02	15.47	15.60	16.60	15.69	16.00	13.94	15.87	15.68	14.32	21.52	28.22	32.40	36.23	31.04
Fe/(Fe+Mg)	0.16	0.17	0.16	0.16	0.16	0.16	0.17	0.16	0.16	0.14	0.16	0.16	0.14	0.22	0.28	0.33	0.36	0.31

Mg # = Mg/(Mg+Fe2+). The formula was calculated on the basis of 4 oxygens. Fe^{2+} was taken as total Fe. ol: olivine; pheno: phenocrysts; mic: microlite.

Appendix A. (Continued)

Sample	Po-21	Po-21	Po-21	Po-21	Po-21	Po-21	Po-21	Po-21	Po-21	Po-21	Po-21	Po-21	Po-21	Po-21	Po-21	Po-21	Po-31	Po-31
Mineral	c2 ol2 pheno rim	c3 ol1 pheno core	c3 ol1 pheno rim	c6 ol1 pheno core	c6 ol1 pheno rim	c7 ol1 pheno core	c7 ol1 pheno rim	c8 ol1 pheno core	c8 ol1 pheno rim	c8 ol1 pheno core	c10 ol1 pheno core	c10 ol1 pheno rim	c10 ol2 pheno core	c10 ol2 pheno rim	c10 ol3 pheno core	c10 ol3 pheno rim	c1 ol1 pheno core	c1 ol1 pheno rim
SiO_2	37.06	39.22	37.51	39.06	38.70	39.50	37.27	38.76	38.12	37.55	37.79	37.79	39.76	39.41	39.06	39.33	38.27	37.94
TiO_2	0.00	0.00	0.05	0.00	0.00	0.00	0.00	0.02	0.00	0.00	0.00	0.00	0.00	0.00	0.00	0.01	0.00	0.00
Al_2O_3	0.01	0.06	0.06	0.03	0.05	0.05	0.05	0.08	0.03	0.06	0.05	0.05	0.05	0.06	0.06	0.07	0.07	0.05
Cr_2O_3	0.00	0.01	0.00	0.00	0.00	0.00	0.00	0.00	0.00	0.00	0.00	0.01	0.02	0.01	0.00	0.00	0.00	0.00
FeO	29.26	17.32	28.12	17.13	20.46	17.28	28.06	21.50	25.19	29.99	25.53	26.12	16.12	17.93	19.33	17.56	22.51	25.07
MnO	0.47	0.25	0.50	0.26	0.32	0.25	0.47	0.33	0.38	0.49	0.41	0.40	0.24	0.29	0.25	0.26	0.47	0.66
MgO	33.44	43.31	34.62	42.83	40.39	42.72	33.77	39.92	36.55	33.27	36.54	36.61	43.66	42.45	41.15	43.18	38.64	36.82
NiO	0.01	0.08	0.09	0.21	0.10	0.11	0.08	0.05	0.05	0.01	0.12	0.08	0.18	0.11	0.10	0.18	0.13	0.07
CaO	0.29	0.33	0.34	0.24	0.28	0.25	0.34	0.35	0.30	0.35	0.31	0.33	0.26	0.29	0.26	0.25	0.32	0.28
Total	100.56	100.61	101.35	99.81	100.32	100.19	100.05	101.05	100.66	101.76	100.76	101.41	100.34	100.56	100.21	100.85	100.52	100.92
Si	0.99	0.99	0.99	1.00	1.00	1.00	1.00	0.99	1.00	1.00	0.99	0.99	1.00	1.00	1.00	0.99	0.99	0.99
Ti	0.00	0.00	0.00	0.00	0.00	0.00	0.00	0.00	0.00	0.00	0.00	0.00	0.00	0.00	0.00	0.00	0.00	0.00
Al	0.00	0.00	0.00	0.00	0.00	0.00	0.00	0.00	0.00	0.00	0.00	0.00	0.00	0.00	0.00	0.00	0.00	0.00
Cr	0.00	0.00	0.00	0.00	0.00	0.00	0.00	0.00	0.00	0.00	0.00	0.00	0.00	0.00	0.00	0.00	0.00	0.00
Fe^{2+}	0.66	0.37	0.62	0.37	0.44	0.37	0.63	0.46	0.55	0.67	0.56	0.57	0.34	0.38	0.41	0.37	0.49	0.55
Mn	0.01	0.01	0.01	0.01	0.01	0.01	0.01	0.01	0.01	0.01	0.01	0.01	0.01	0.01	0.01	0.01	0.01	0.01
Mg	1.34	1.63	1.37	1.63	1.55	1.61	1.35	1.53	1.43	1.32	1.43	1.43	1.64	1.60	1.57	1.62	1.50	1.44
Ni	0.00	0.00	0.00	0.00	0.00	0.00	0.00	0.00	0.00	0.00	0.00	0.00	0.00	0.00	0.00	0.00	0.00	0.00
Ca	0.01	0.01	0.01	0.01	0.01	0.01	0.01	0.01	0.01	0.01	0.01	0.01	0.01	0.01	0.01	0.01	0.01	0.01
Total	3.01	3.01	3.01	3.00	3.00	3.00	3.00	3.00	3.00	3.00	3.01	3.01	3.00	3.00	3.00	3.01	3.00	3.01
Mg#	0.67	0.82	0.69	0.82	0.78	0.82	0.68	0.77	0.72	0.66	0.72	0.71	0.83	0.81	0.79	0.81	0.75	0.72
Fo	66.73	81.46	68.32	81.44	77.60	81.29	67.85	76.53	71.82	66.04	71.52	71.11	82.63	80.60	78.93	81.19	74.98	71.83
Fa	32.74	18.27	31.12	18.27	22.05	18.44	31.62	23.12	27.76	33.40	28.02	28.45	17.12	19.09	20.80	18.52	24.50	27.44
Fe/(Fe+Mg)	0.33	0.18	0.31	0.18	0.22	0.18	0.32	0.23	0.28	0.34	0.28	0.29	0.17	0.19	0.21	0.19	0.25	0.28

Mg # = Mg / (Mg+Fe2+). The formula was calculated on the basis of 4 oxygens. Fe^{2+} was taken as total Fe. ol: olivine; pheno: phenocrysts; mic: microlite.

Appendix A. (Continued)

Sample	Po-31	Po-31	Po-31	Po-31	Po-31	Po-31	Po-31	Po-31	Po-31	Po-31	Po-31	Po-31	Po-31	Po-31	Po-31	Po-31	Po-31	Po-21
Mineral	c1 ol1 pheno core	c1 ol1 pheno rim	c2 ol1 pheno core	c2 ol1 pheno rim	c3 ol1 pheno core	c3 ol1 pheno rim	c4 ol1 pheno core	c4 ol1 pheno rim	c4 ol2 pheno core	c4 ol2 pheno rim	c5 ol1 pheno core	c5 ol1 pheno rim	c6 ol1 pheno core	c6 ol1 pheno rim	c7 ol1 pheno core	c7 ol1 pheno rim	c7 ol2 pheno core	c7 ol2 pheno rim	c3 ol1 mik
SiO_2	38.12	37.60	38.10	38.08	38.71	38.22	38.30	38.18	38.37	37.90	38.36	38.32	37.81	37.95	38.34	37.95	38.45	38.41	35.35
TiO_2	0.04	0.04	0.00	0.00	0.00	0.01	0.00	0.00	0.00	0.00	0.00	0.00	0.00	0.00	0.01	0.00	0.00	0.03	0.02
Al_2O_3	0.00	0.02	0.05	0.04	0.03	0.05	0.05	0.04	0.08	0.00	0.03	0.02	0.10	0.05	0.03	0.04	0.03	0.01	0.03
Cr_2O_3	0.00	0.00	0.00	0.00	0.00	0.00	0.00	0.00	0.00	0.01	0.00	0.00	0.00	0.00	0.00	0.00	0.00	0.00	0.00
FeO	24.56	24.50	23.33	23.93	21.13	24.63	23.01	24.60	23.21	24.55	21.19	24.76	24.17	24.64	24.10	24.07	23.01	24.21	38.17
MnO	0.54	0.66	0.56	0.55	0.43	0.59	0.51	0.59	0.53	0.61	0.46	0.60	0.52	0.65	0.56	0.56	0.51	0.59	0.65
MgO	36.24	36.87	37.52	37.09	39.64	36.79	37.71	36.53	37.55	37.02	39.27	37.08	37.51	36.45	37.98	36.96	38.53	37.38	26.41
NiO	0.17	0.07	0.13	0.10	0.14	0.13	0.10	0.09	0.11	0.05	0.15	0.10	0.12	0.02	0.10	0.12	0.14	0.09	0.06
CaO	0.29	0.33	0.29	0.32	0.24	0.35	0.30	0.29	0.31	0.28	0.28	0.28	0.23	0.32	0.29	0.29	0.35	0.24	0.39
Total	99.97	100.13	100.00	100.14	100.39	100.78	100.04	100.32	100.28	100.50	99.86	101.17	100.47	100.10	101.43	100.02	101.10	101.06	101.10
Si	1.00	0.99	1.00	1.00	1.00	1.00	1.00	1.00	1.00	0.99	1.00	1.00	0.99	1.00	0.99	1.00	1.00	1.00	0.89
Ti	0.00	0.00	0.00	0.00	0.00	0.00	0.00	0.00	0.00	0.00	0.00	0.00	0.00	0.00	0.00	0.00	0.00	0.00	0.00
Al	0.00	0.00	0.00	0.00	0.00	0.00	0.00	0.00	0.00	0.00	0.00	0.00	0.00	0.00	0.00	0.00	0.00	0.00	0.00
Cr	0.00	0.00	0.00	0.00	0.00	0.00	0.00	0.00	0.00	0.00	0.00	0.00	0.00	0.00	0.00	0.00	0.00	0.00	0.00
Fe^{2+}	0.54	0.54	0.51	0.53	0.46	0.54	0.50	0.54	0.51	0.54	0.46	0.54	0.53	0.54	0.52	0.53	0.50	0.53	0.80
Mn	0.01	0.01	0.01	0.01	0.01	0.01	0.01	0.01	0.01	0.01	0.01	0.01	0.01	0.01	0.01	0.01	0.01	0.01	0.01
Mg	1.42	1.45	1.47	1.45	1.53	1.43	1.47	1.43	1.46	1.45	1.52	1.44	1.46	1.43	1.47	1.45	1.49	1.45	0.99
Ni	0.00	0.00	0.00	0.00	0.00	0.00	0.00	0.00	0.00	0.00	0.00	0.00	0.00	0.00	0.00	0.00	0.00	0.00	0.00
Ca	0.01	0.01	0.01	0.01	0.01	0.01	0.01	0.01	0.01	0.01	0.01	0.01	0.01	0.01	0.01	0.01	0.01	0.01	0.01
Total	2.99	3.01	3.00	3.00	3.00	3.00	3.00	3.00	3.00	3.00	3.00	3.00	3.01	3.00	3.01	3.00	3.00	3.00	2.71
Mg#	0.72	0.73	0.74	0.73	0.77	0.73	0.75	0.73	0.74	0.73	0.77	0.73	0.73	0.73	0.74	0.73	0.75	0.73	0.55
Fo	72.02	72.31	73.68	72.98	76.62	72.21	74.08	72.11	73.82	72.39	76.37	72.26	73.03	71.98	73.30	72.79	74.49	72.87	54.80
Fa	27.38	26.95	25.70	26.40	22.90	27.12	25.35	27.23	25.59	26.93	23.12	27.07	26.39	27.29	26.09	26.59	24.95	26.47	44.43
Fe/(Fe+Mg)	0.28	0.27	0.26	0.27	0.23	0.27	0.25	0.27	0.26	0.27	0.23	0.27	0.27	0.27	0.26	0.27	0.25	0.27	0.45

Mg # = Mg / (Mg+Fe^{2+}). The formula was calculated on the basis of 4 oxygens. Fe^{2+} was taken as total Fe. ol: olivine; pheno: phenocrysts; mic: microlite.

Appendix B.

Electron microprobe analysis results of orthopyroxene phenocrysts from Late Miocene basic volcanic rocks.

Sample	*Po-6*	Po-6	*Po-6*	Po-6	Po-6	Po-6	*Po-6*	Po-6	Po-35	Po-35
Mineral	*c2*	c2	*c3*	c3	c5	c5	*c9*	c9	c9	c9
	opx-1	opx-1	*opx-1*	opx-1	opx-1	opx-1	*opx-1*	opx-1	opx -1	opx-1
	pheno	pheno	*pheno*	pheno	pheno	pheno	*pheno*	pheno	pheno	pheno
	core	rim	*core*	mid	core	rim	*core*	rim	core	rim
SiO_2	*55.20*	56.13	*53.58*	52.98	55.50	55.44	*55.08*	54.86	54.39	55.11
TiO_2	*0.16*	0.15	*0.22*	0.27	0.17	0.20	*0.24*	0.20	0.23	0.05
Al_2O_3	*1.70*	1.10	*1.79*	2.67	1.76	1.83	*1.92*	2.11	3.67	1.30
Cr_2O_3	*0.15*	0.13	*0.00*	0.00	0.18	0.16	*0.15*	0.20	0.02	0.17
FeO	*9.23*	9.20	*15.42*	14.76	9.76	9.79	*9.81*	9.88	10.74	10.70
MnO	*0.27*	0.24	*0.45*	0.26	0.25	0.23	*0.27*	0.21	0.21	0.23
MgO	*30.42*	30.74	*26.53*	26.74	30.08	30.04	*30.24*	29.63	28.85	30.34
CaO	*2.10*	1.97	*1.28*	1.36	1.98	1.91	*1.78*	1.92	1.42	1.34
Na_2O	*0.02*	0.04	*0.01*	0.01	0.06	0.04	*0.02*	0.03	0.07	0.04
K_2O	*0.00*	0.00	*0.00*	0.00	0.00	0.01	*0.00*	0.03	0.02	0.00
Total	*99.24*	99.70	*99.28*	99.05	99.74	99.65	*99.52*	99.07	99.63	99.28
Si	*1.96*	1.98	*1.95*	1.93	1.96	1.96	*2.06*	2.05	1.93	1.96
Ti	*0.00*	0.00	*0.01*	0.01	0.00	0.01	*0.01*	0.01	0.01	0.00
Al	*0.07*	0.05	*0.08*	0.11	0.07	0.08	*0.08*	0.09	0.15	0.05
Cr	*0.00*	0.00	*0.00*	0.00	0.01	0.00	*0.00*	0.01	0.00	0.00
Fe^{2+}	*0.27*	0.27	*0.47*	0.45	0.29	0.29	*0.31*	0.31	0.32	0.32
Mn	*0.01*	0.01	*0.01*	0.01	0.01	0.01	*0.01*	0.01	0.01	0.01
Mg	*1.61*	1.61	*1.44*	1.45	1.58	1.58	*1.69*	1.65	1.52	1.61
Ca	*0.08*	0.07	*0.05*	0.05	0.07	0.07	*0.07*	0.08	0.05	0.05
Na	*0.00*	0.00	*0.00*	0.00	0.00	0.00	*0.00*	0.00	0.01	0.00
K	*0.00*	0.00	*0.00*	0.00	0.00	0.00	*0.00*	0.00	0.00	0.00
Total	*4.00*	4.00	*4.01*	4.01	4.00	4.00	*4.23*	4.20	3.99	4.01
Mg#	*0.85*	0.86	*0.75*	0.76	0.85	0.85	*0.85*	0.84	0.83	0.83
Wo	*4*	4	*3*	3	4	4	*3*	4	3	3
En	*82*	82	*73*	74	81	81	*81*	81	80	81
Fs	*14*	14	*24*	23	15	15	*14*	15	17	16
Total	*100*	100	*100*	100	100	100	*100*	100	100	100

Mg # = Mg / (Mg+Fe2+). The formula was calculated on the basis of 6 oxygens. Fe^{2+} was taken as total Fe. opx: orthopyroxene; pheno: phenocrysts; mid.: middle Italic columns were used for P-T calculations.

Appendix C.

Electron microprobe analysis results of clinopyroxene phenocrysts from Late Miocene basic volcanic rocks.

Sample	Po-6	Po-6	Po-6	Po-6	Po-6	Po-6	Po-6	Po-6	Po-6	Po-17	Po-17	Po-17	Po-17	Po-17	Po-17	Po-17	Po-17	Po-17
Mineral	c5	c7	c8	c8	c8	c8	c8	c11	c11	c1	c1	c3	c3	c5	c5	c5	c5	c6
	cpx-2	cpx-1	cpx-1	cpx-1	cpx-1	cpx-2	cpx-2	cpx-1	cpx-3	cpx-1	cpx-1	cpx-1	cpx-1	cpx-1	cpx-1	cpx-2	cpx-2	cpx-1
	pheno	pheno	pheno	pheno	pheno	pheno	pheno	pheno	pheno	pheno	pheno	pheno	pheno	pheno	pheno	pheno	pheno	pheno
	core	rim	mid.	mid.	rim	core	rim	core	rim	core	rim	core	rim	core	rim	core	mid.	mid.
SiO_2	*51.44*	52.12	*50.60*	*52.53*	52.77	*51.15*	51.78	*51.85*	51.58	*50.91*	50.62	*51.10*	50.86	*51.81*	50.57	*51.33*	*50.69*	*50.24*
TiO_2	*0.43*	0.31	*0.86*	*0.36*	0.36	*0.61*	0.39	*0.38*	0.42	*0.52*	0.60	*0.66*	0.55	*0.66*	0.77	*0.72*	*0.77*	*0.64*
Al_2O_3	*3.42*	2.54	*3.57*	*2.28*	2.53	*2.64*	3.08	*2.60*	2.89	*3.10*	3.54	*2.92*	3.45	*2.32*	3.60	*2.76*	*3.24*	*3.80*
Cr_2O_3	*0.25*	0.27	*0.00*	*0.36*	0.23	*0.06*	0.24	*0.22*	0.39	*0.27*	0.18	*0.00*	0.30	*0.02*	0.40	*0.00*	*0.00*	*0.31*
FeO	*6.52*	6.21	*8.21*	*6.09*	5.70	*7.07*	6.80	*6.74*	6.13	*6.66*	6.60	*7.18*	6.47	*6.77*	6.49	*7.62*	*7.88*	*7.14*
MnO	*0.19*	0.18	*0.26*	*0.18*	0.19	*0.21*	0.18	*0.17*	0.17	*0.17*	0.20	*0.23*	0.18	*0.25*	0.17	*0.23*	*0.27*	*0.17*
MgO	*16.89*	17.13	*15.68*	*17.68*	17.35	*16.52*	17.19	*16.65*	16.67	*16.15*	15.78	*15.75*	16.18	*16.52*	15.71	*16.00*	*15.77*	*15.68*
CaO	*19.82*	19.90	*19.13*	*19.51*	20.12	*20.37*	18.95	*20.23*	20.35	*21.21*	21.13	*20.67*	20.80	*20.26*	21.20	*19.74*	*19.67*	*20.42*
Na_2O	*0.38*	0.38	*0.71*	*0.31*	0.38	*0.49*	0.39	*0.34*	0.34	*0.41*	0.40	*0.53*	0.40	*0.57*	0.37	*0.83*	*0.86*	*0.60*
K_2O	*0.00*	0.00	*0.01*	*0.00*	0.00	*0.00*	0.00	*0.00*	0.00	*0.00*	0.01	*0.00*	0.00	*0.00*	0.00	*0.00*	*0.00*	*0.00*
Total	*99.33*	99.04	*99.03*	*99.29*	99.64	*99.12*	98.99	*99.18*	98.94	*99.40*	99.06	*99.04*	99.18	*99.17*	99.27	*99.22*	*99.15*	*99.00*
Si	*1.90*	1.93	*1.89*	*1.96*	1.97	*1.91*	1.94	*1.94*	1.93	*1.89*	1.89	*1.91*	1.89	*1.92*	1.88	*1.91*	*1.89*	*1.88*
Ti	*0.01*	0.01	*0.02*	*0.01*	0.01	*0.02*	0.01	*0.01*	0.01	*0.01*	0.02	*0.02*	0.02	*0.02*	0.02	*0.02*	*0.02*	*0.02*
Al	*0.15*	0.11	*0.16*	*0.10*	0.11	*0.12*	0.14	*0.11*	0.13	*0.14*	0.16	*0.13*	0.15	*0.10*	0.16	*0.12*	*0.14*	*0.17*
Cr	*0.01*	0.01	*0.00*	*0.01*	0.01	*0.00*	0.01	*0.01*	0.01	*0.01*	0.01	*0.00*	0.01	*0.00*	0.01	*0.00*	*0.00*	*0.01*
Fe^{2+}	*0.20*	0.19	*0.26*	*0.19*	0.18	*0.22*	0.21	*0.21*	0.19	*0.21*	0.21	*0.22*	0.20	*0.21*	0.20	*0.24*	*0.25*	*0.22*
Mn	*0.01*	0.01	*0.01*	*0.01*	0.01	*0.01*	0.01	*0.01*	0.01	*0.01*	0.01	*0.01*	0.01	*0.01*	0.01	*0.01*	*0.01*	*0.01*
Mg	*0.93*	0.95	*0.87*	*0.99*	0.97	*0.92*	0.96	*0.93*	0.93	*0.90*	0.88	*0.88*	0.90	*0.92*	0.87	*0.89*	*0.88*	*0.87*
Ca	*0.79*	0.79	*0.77*	*0.78*	0.81	*0.82*	0.76	*0.81*	0.82	*0.85*	0.84	*0.83*	0.83	*0.81*	0.85	*0.79*	*0.79*	*0.82*
Na	*0.03*	0.03	*0.05*	*0.02*	0.03	*0.04*	0.03	*0.02*	0.02	*0.03*	0.03	*0.04*	0.03	*0.04*	0.03	*0.06*	*0.06*	*0.04*
K	*0.00*	0.00	*0.00*	*0.00*	0.00	*0.00*	0.00	*0.00*	0.00	*0.00*	0.00	*0.00*	0.00	*0.00*	0.00	*0.00*	*0.00*	*0.00*
Total	*4.02*	4.02	*4.03*	*4.07*	4.09	*4.05*	4.05	*4.05*	4.05	*4.03*	4.03	*4.03*	4.03	*4.03*	4.02	*4.04*	*4.04*	*4.04*
Mg#	*0.82*	0.83	*0.77*	*0.84*	0.84	*0.81*	0.82	*0.81*	0.83	*0.81*	0.81	*0.80*	0.82	*0.81*	0.81	*0.79*	*0.78*	*0.80*
Wo	*40.84*	40.86	*40.26*	*39.83*	41.21	*41.58*	39	*41.50*	42.02	*43.30*	43.69	*42.78*	42.92	*41.60*	43.95	*41.05*	*41.06*	*42.63*
En	*48.42*	48.94	*45.93*	*50.25*	49.44	*46.91*	50	*47.52*	47.90	*45.90*	45.41	*45.34*	46.45	*47.21*	45.33	*46.31*	*45.81*	*45.57*
Fs	*10.74*	10.20	*13.81*	*9.92*	9.35	*11.51*	11	*10.98*	10.08	*10.80*	10.90	*11.88*	10.63	*11.19*	10.72	*12.63*	*13.13*	*11.80*
Total	*100*	100	*100*	*100*	100	*100*	100	*100*	100	*100*	100	*100*	100	*100*	100	*100*	*100*	*100*

Mg # = Mg/(Mg+Fe2+). The formula was calculated on the basis of 6 oxygens. Fe^{2+} was taken as total Fe. cpx: clinopyroxene; pheno: phenocrysts, mid.: middle. Italic columns were used for P-T calculations.

Appendix C.

(Continued)

Sample	Po-17	*Po-21*	Po-21	*Po-21*	Po-21	*Po-21*	Po-21	*Po-21*	Po-21	*Po-35*	Po-35	*Po-35*	Po-35
Mineral	c6	*c1*	c1	*c4*	c4	*c9*	c9	*c10*	c10	*c3*	c3	*c11*	c11
	cpx-1	*cpx-2*	cpx-2	*cpx-1*	cpx-1	*cpx-1*	cpx-1	*cpx-1*	cpx-1	*cpx-1*	cpx-2	*cpx-1*	cpx-1
	pheno	*pheno*	pheno	*pheno*	pheno	*pheno*	pheno	*pheno*	pheno	*pheno*	pheno	*pheno*	pheno
	rim	*core*	rim	*core*	rim	*core*	rim	*core*	rim	*core*	rim	*core*	rim
SiO_2	50.68	*49.56*	49.83	*50.01*	51.84	*50.80*	50.96	*51.92*	52.04	*52.64*	51.19	*51.94*	51.38
TiO_2	0.64	*1.09*	1.70	*1.20*	0.65	*1.12*	1.26	*0.84*	0.90	*0.29*	0.50	*0.46*	0.45
Al_2O_3	3.80	*3.86*	2.88	*3.61*	1.78	*3.17*	2.93	*1.82*	1.68	*2.52*	3.07	*3.05*	3.05
Cr_2O_3	0.29	*0.65*	0.00	*0.51*	0.24	*0.24*	0.06	*0.06*	0.02	*0.31*	0.02	*0.24*	0.00
FeO	7.35	*7.18*	9.56	*7.21*	7.60	*7.39*	8.10	*7.64*	8.57	*5.31*	8.44	*5.87*	7.89
MnO	0.18	*0.20*	0.25	*0.14*	0.19	*0.15*	0.22	*0.19*	0.22	*0.16*	0.22	*0.15*	0.18
MgO	15.44	*14.96*	14.14	*14.80*	16.76	*14.79*	14.76	*15.34*	15.50	*16.82*	15.09	*16.37*	15.61
CaO	20.13	*21.34*	20.61	*21.34*	20.22	*21.64*	21.36	*21.20*	20.65	*20.92*	20.46	*21.13*	20.05
Na_2O	0.54	*0.36*	0.36	*0.40*	0.24	*0.32*	0.34	*0.35*	0.30	*0.32*	0.44	*0.42*	0.43
K_2O	0.00	*0.01*	0.01	*0.00*	0.00	*0.00*	0.00	*0.00*	0.00	*0.00*	0.00	*0.01*	0.00
Total	99.04	*99.21*	99.34	*99.22*	99.53	*99.62*	99.99	*99.36*	99.88	*99.28*	99.44	*99.62*	99.04
Si	1.89	*1.86*	1.88	*1.87*	1.93	*1.89*	1.90	*1.94*	1.94	*1.94*	1.91	*1.92*	1.92
Ti	0.02	*0.03*	0.05	*0.03*	0.02	*0.03*	0.04	*0.02*	0.03	*0.01*	0.01	*0.01*	0.01
Al	0.17	*0.17*	0.13	*0.16*	0.08	*0.14*	0.13	*0.08*	0.07	*0.11*	0.14	*0.13*	0.13
Cr	0.01	*0.02*	0.00	*0.02*	0.01	*0.01*	0.00	*0.00*	0.00	*0.01*	0.00	*0.01*	0.00
Fe^{2+}	0.23	*0.23*	0.30	*0.23*	0.24	*0.23*	0.25	*0.24*	0.27	*0.16*	0.26	*0.18*	0.25
Mn	0.01	*0.01*	0.01	*0.00*	0.01	*0.00*	0.01	*0.01*	0.01	*0.00*	0.01	*0.00*	0.01
Mg	0.86	*0.84*	0.80	*0.83*	0.93	*0.82*	0.82	*0.85*	0.86	*0.92*	0.84	*0.90*	0.87
Ca	0.80	*0.86*	0.83	*0.86*	0.80	*0.86*	0.85	*0.85*	0.82	*0.83*	0.82	*0.83*	0.80
Na	0.04	*0.03*	0.03	*0.03*	0.02	*0.02*	0.02	*0.03*	0.02	*0.02*	0.03	*0.03*	0.03
K	0.00	*0.00*	0.00	*0.00*	0.00	*0.00*	0.00	*0.00*	0.00	*0.00*	0.00	*0.00*	0.00
Total	4.02	*4.03*	4.02	*4.02*	4.02	*4.01*	4.02	*4.01*	4.01	*4.01*	4.02	*4.02*	4.02
Mg#	0.79	*0.79*	0.72	*0.79*	0.80	*0.78*	0.76	*0.78*	0.76	*0.85*	0.76	*0.83*	0.78
Wo	42.42	*44.57*	43.03	*44.79*	40.78	*45*	44.15	*43.59*	42.09	*43.06*	42.46	*43.50*	41.73
En	45.27	*43.48*	41.07	*43.24*	47.02	*43*	42.47	*43.88*	43.96	*48.17*	43.59	*46.88*	45.21
Fs	12.30	*11.94*	15.91	*11.98*	12.21	*12*	13.38	*12.53*	13.95	*8.78*	13.95	*9.62*	13.06
Total	100	*100*	100	*100*	100	*100*	100	*100*	100	*100*	100	*100*	100

Mg # = Mg/(Mg+Fe2+). The formula was calculated on the basis of 6 oxygens. Fe^{2+} was taken as total Fe. cpx: clinopyroxene; pheno: phenocrysts, mid.: middle. Italic columns were used for P-T calculations.

Appendix D.

Electron microprobe analysis results of plagioclase phenocrysts and microlite from Late Miocene basic volcanic rocks

Sample	Po-6	Po-6	Po-6	Po-6	Po-6	Po-6	Po-6	Po-6	Po-6	Po-6	Po-6	Po-6	Po-6	Po-6	Po-6	Po-6	Po-6	Po-6
Mineral	c1	c1	c1	c1	c2	c2	c2	c2	c4	c4	c4	c4	c7	c7	c9	c9	c10	c10
	pl-1	pl-1	pl-2	pl-2	pl-1	pl-1	pl-2	pl-2	pl-1	pl-1	pl-2	pl-2	pl-1	pl-1	pl-1	pl-1	pl-1	pl-1
	pheno	pheno	pheno	pheno	pheno	pheno	pheno	pheno	pheno	pheno	pheno	pheno	pheno	pheno	pheno	pheno	pheno	pheno
	core	rim	core	rim	core	rim	core	rim	core	rim	core	rim	core	rim	core	rim	core	rim
SiO_2	53.69	52.62	52.47	54.61	52.68	53.23	52.46	52.63	53.61	53.83	52.39	54.29	52.35	53.45	52.91	53.57	52.29	52.87
Al_2O_3	28.37	29.21	29.40	27.85	29.14	29.06	29.36	29.19	28.72	28.65	29.41	28.45	29.13	28.75	29.06	28.32	29.67	29.30
FeO	0.84	0.86	0.85	1.01	0.79	0.88	0.95	0.88	0.92	0.94	0.85	0.94	0.80	0.77	0.87	1.04	0.79	0.95
CaO	11.60	12.45	12.53	10.76	12.55	12.09	12.29	12.29	11.74	11.35	12.36	11.20	12.36	11.59	12.27	11.77	12.47	12.05
Na_2O	4.71	4.18	4.12	5.17	4.11	4.46	4.14	4.39	4.46	4.53	4.12	4.59	4.17	4.53	4.40	4.46	4.03	4.19
K_2O	0.32	0.28	0.26	0.37	0.28	0.27	0.31	0.27	0.32	0.34	0.26	0.32	0.25	0.32	0.28	0.33	0.25	0.24
BaO	0.00	0.00	0.00	0.00	0.00	0.00	0.00	0.00	0.00	0.00	0.00	0.00	0.00	0.00	0.00	0.00	0.00	0.00
Total	99.53	99.59	99.64	99.77	99.54	99.98	99.52	99.64	99.77	99.64	99.38	99.80	99.06	99.40	99.80	99.48	99.49	99.60
Si	9.70	9.50	9.48	9.86	9.51	9.61	9.47	9.51	9.68	9.72	9.46	9.81	9.46	9.65	9.56	9.68	9.44	9.55
Al	6.04	6.22	6.26	5.93	6.20	6.19	6.25	6.21	6.11	6.10	6.26	6.06	6.20	6.12	6.19	6.03	6.32	6.24
Fe^{2+}	0.13	0.13	0.13	0.15	0.12	0.13	0.14	0.13	0.14	0.14	0.13	0.14	0.12	0.12	0.13	0.16	0.12	0.14
Ca	2.24	2.41	2.42	2.08	2.43	2.34	2.38	2.38	2.27	2.20	2.39	2.17	2.39	2.24	2.38	2.28	2.41	2.33
Na	1.65	1.46	1.44	1.81	1.44	1.56	1.45	1.54	1.56	1.59	1.44	1.61	1.46	1.59	1.54	1.56	1.41	1.47
K	0.07	0.06	0.06	0.09	0.06	0.06	0.07	0.06	0.07	0.08	0.06	0.07	0.06	0.07	0.07	0.08	0.06	0.06
Ba	0.00	0.00	0.00	0.00	0.00	0.00	0.00	0.00	0.00	0.00	0.00	0.00	0.00	0.00	0.00	0.00	0.00	0.00
Total	19.83	19.79	19.79	19.92	19.77	19.89	19.77	19.83	19.84	19.82	19.74	19.85	19.69	19.79	19.85	19.77	19.76	19.78
An	57	61	62	52	62	59	61	60	58	57	61	56	61	57	60	58	62	61
Ab	42	37	37	45	37	39	37	39	40	41	37	42	37	41	39	40	36	38
Or	2	2	2	2	2	2	2	2	2	2	2	2	1	2	2	2	1	1
Total	100	100	100	100	100	100	100	100	100	100	100	100	100	100	100	100	100	100

The formula was calculated on the basis of 32 oxygens. Fe^{2+} was taken as total Fe. pl: plagioclase; pheno: phenocrysts; mid.: middle.

Appendix D. (Continued).

Sample	Po-6	Po-6	Po-17	Po-17	Po-17	Po-17	Po-17	Po-17	Po-17	Po-17	Po-17	Po-17	Po-17	Po-17	Po-21	Po-21	Po-21	Po-21
Mineral	c11	c11	c2	c2	c3	c3	c3	c3	c6	c6	c7	c8	c9	c9	c3	c3	c5	c5
	pl-1	pl-1	pl-1	pl-1	pl-1	pl-1	pl-2	pl-2	pl-1	pl-1	pl-1	pl-1	pl-1	pl-1	pl-1	pl-1	pl-1	pl-1
	pheno	pheno	pheno	pheno	pheno	pheno	pheno	pheno	pheno	pheno	pheno	pheno	pheno	pheno	pheno	pheno	pheno	pheno
	core	rim	core	rim	core	rim	core	rim	core	rim	rim	rim	core	rim	core	rim	core	rim
SiO_2	53.66	53.49	52.44	52.19	54.93	52.57	55.06	54.89	52.24	55.13	51.70	54.05	55.57	52.00	48.30	54.19	50.46	49.86
Al_2O_3	28.58	29.20	29.48	29.74	27.54	29.21	26.99	27.70	29.62	26.89	29.65	27.73	27.52	29.42	32.61	28.30	31.35	32.10
FeO	0.77	0.84	0.83	0.77	0.65	0.68	0.93	0.87	0.82	1.42	0.86	1.19	0.88	0.98	0.59	0.85	0.54	0.56
CaO	11.25	12.10	12.50	12.54	10.44	11.70	10.05	10.46	12.36	10.25	12.32	10.73	9.94	12.23	15.92	10.60	14.31	14.60
Na_2O	4.58	4.35	4.24	4.07	5.11	4.41	5.34	5.16	4.20	5.41	4.16	5.05	5.55	4.26	2.55	5.27	3.39	3.07
K_2O	0.32	0.30	0.37	0.34	0.49	0.39	0.58	0.50	0.33	0.57	0.32	0.52	0.61	0.38	0.09	0.28	0.08	0.09
BaO	0.00	0.00	0.00	0.00	0.00	0.00	0.00	0.00	0.00	0.00	0.00	0.00	0.00	0.00	0.00	0.00	0.00	0.00
Total	99.16	100.28	99.86	99.64	99.16	98.96	98.94	99.59	99.58	99.67	99.00	99.28	100.07	99.26	100.05	99.49	100.13	100.28
Si	9.69	9.66	9.47	9.43	9.92	9.49	9.94	9.91	9.44	9.96	9.34	9.76	10.04	9.39	8.87	9.87	9.20	9.09
Al	6.08	6.22	6.28	6.33	5.86	6.22	5.74	5.90	6.31	5.72	6.31	5.90	5.86	6.26	7.05	6.07	6.74	6.89
Fe^{2+}	0.12	0.13	0.13	0.12	0.10	0.10	0.14	0.13	0.12	0.21	0.13	0.18	0.13	0.15	0.09	0.13	0.08	0.08
Ca	2.18	2.34	2.42	2.43	2.02	2.26	1.95	2.02	2.39	1.98	2.38	2.08	1.92	2.37	3.13	2.07	2.80	2.85
Na	1.60	1.52	1.48	1.42	1.79	1.54	1.87	1.81	1.47	1.89	1.46	1.77	1.94	1.49	0.91	1.86	1.20	1.08
K	0.07	0.07	0.09	0.08	0.11	0.09	0.13	0.11	0.08	0.13	0.07	0.12	0.14	0.09	0.02	0.07	0.02	0.02
Ba	0.00	0.00	0.00	0.00	0.00	0.00	0.00	0.00	0.00	0.00	0.00	0.00	0.00	0.00	0.00	0.00	0.00	0.00
Total	19.75	19.94	19.86	19.80	19.80	19.71	19.78	19.89	19.80	19.90	19.69	19.81	20.03	19.75	20.07	20.06	20.04	20.02
An	56	60	61	62	51	58	49	51	61	50	61	52	48	60	77	52	69	72
Ab	42	39	37	36	46	40	47	46	37	47	37	45	48	38	22	46	30	27
Or	2	2	2	2	3	2	3	3	2	3	2	3	4	2	1	2	1	1
Total	100	100	100	100	100	100	100	100	100	100	100	100	100	100	100	100	100	100

The formula was calculated on the basis of 32 oxygens. Fe^{2+} was taken as total Fe. pl: plagioclase; pheno: phenocrysts; mid.: middle.

Appendix D. (Continued).

Sample	Po-21	Po-21	Po-21	Po-21	Po-35	Po-35	Po-35	Po-35	Po-35	Po-35	Po-35	Po-35	Po-35	Po-35	Po-35	Po-35	Po-35	Po-35
Mineral	c7	c7	c12	c12	c1	c1	c1	c1	c2	c2	c2	c2	c2	c3	c3	c4	c4	c4
	pl-1	pl-1	pl-1	pl-1	pl-1	pl-1	pl-3	pl-3	pl-1	pl-1	pl-1	pl-1	pl-1	pl-1	pl-1	pl-1	pl-2	pl-2
	pheno	pheno	pheno	pheno	pheno	pheno	pheno	pheno	pheno	pheno	pheno	pheno	pheno	pheno	pheno	pheno	pheno	pheno
	core	rim	core	rim	core	rim	core	rim	core	mid-1	mid-2	mid-3	rim	core	rim	core	core	rim
SiO_2	51.23	58.08	49.53	52.03	54.60	54.10	51.81	53.19	57.00	55.72	57.98	58.31	53.33	55.18	57.81	55.48	54.74	56.37
Al_2O_3	30.64	25.86	31.49	30.11	28.73	29.11	30.06	28.96	27.30	27.61	26.52	26.40	28.71	28.39	26.64	28.13	28.41	27.72
FeO	0.68	0.74	0.38	0.65	0.42	0.34	0.40	0.50	0.23	0.32	0.29	0.23	0.54	0.36	0.26	0.38	0.34	0.32
CaO	13.60	7.69	14.83	12.74	11.08	11.24	13.00	11.80	9.12	9.63	8.02	8.10	12.19	10.38	8.55	10.08	10.73	9.36
Na_2O	3.70	6.81	3.03	4.01	5.10	4.97	4.07	4.47	6.23	5.76	6.56	6.44	4.39	5.40	6.35	5.43	5.24	5.93
K_2O	0.15	0.58	0.10	0.19	0.21	0.19	0.15	0.19	0.29	0.28	0.34	0.43	0.26	0.24	0.32	0.28	0.25	0.27
BaO	0.00	0.00	0.00	0.00	0.00	0.00	0.00	0.00	0.00	0.00	0.00	0.00	0.00	0.00	0.00	0.00	0.00	0.00
Total	99.99	99.75	99.38	99.74	100.15	99.95	99.49	99.12	100.17	99.32	99.70	99.91	99.42	99.94	99.94	99.77	99.72	99.98
Si	9.34	10.46	9.11	9.49	9.86	9.77	9.36	9.61	10.29	10.06	10.47	10.53	9.63	9.97	10.44	10.02	9.89	10.18
Al	6.59	5.49	6.83	6.47	6.12	6.20	6.40	6.16	5.81	5.88	5.64	5.62	6.11	6.04	5.67	5.99	6.05	5.90
Fe^{2+}	0.10	0.11	0.06	0.10	0.06	0.05	0.06	0.08	0.03	0.05	0.04	0.03	0.08	0.05	0.04	0.06	0.05	0.05
Ca	2.66	1.48	2.92	2.49	2.14	2.17	2.51	2.28	1.76	1.86	1.55	1.57	2.36	2.01	1.65	1.95	2.08	1.81
Na	1.31	2.38	1.08	1.42	1.79	1.74	1.42	1.56	2.18	2.02	2.30	2.25	1.54	1.89	2.22	1.90	1.84	2.08
K	0.03	0.13	0.02	0.04	0.05	0.04	0.04	0.04	0.07	0.06	0.08	0.10	0.06	0.05	0.07	0.06	0.06	0.06
Ba	0.00	0.00	0.00	0.00	0.00	0.00	0.00	0.00	0.00	0.00	0.00	0.00	0.00	0.00	0.00	0.00	0.00	0.00
Total	20.03	20.05	20.03	20.01	20.02	19.98	19.79	19.74	20.15	19.93	20.09	20.11	19.78	20.02	20.10	19.98	19.96	20.08
An	66	37	73	63	54	55	63	59	44	47	40	40	60	51	42	50	52	46
Ab	33	60	27	36	45	44	36	40	54	51	58	58	39	48	56	48	46	53
Or	1	3	0	1	1	1	1	1	2	2	2	2	1	1	2	2	2	1
Total	100	100	100	100	100	100	100	100	100	100	100	100	100	100	100	100	100	100

The formula was calculated on the basis of 32 oxygens. Fe^{2+} was taken as total Fe. pl: plagioclase; pheno: phenocrysts; mid.: middle.

Appendix D. (Continued).

Sample	Po-35	Po-35	Po-35	Po-35	Po-35	Po-35	Po-35	Po-35	Po-35	Po-35	Po-35	Po-35	Po-35
Mineral	c5	c5	c5	c5	c6	c6	c6	c6	c7	c7	c7	c7	c9
	pl-1	pl-1	pl-2	pl-2	pl-1	pl-1	pl-2	pl-2	pl-1	pl-1	pl-2	pl-2	pl-1
	pheno	pheno	pheno	pheno	pheno	pheno	pheno	pheno	pheno	pheno	pheno	pheno	pheno
	core	rim	core	rim	core	rim	core	rim	core	rim	core	rim	rim
SiO_2	48.68	52.20	54.42	59.93	52.80	52.12	57.82	54.71	51.85	51.35	52.51	51.94	51.64
Al_2O_3	32.27	30.03	28.80	25.41	29.82	29.51	26.49	28.53	29.77	30.12	29.56	30.28	29.77
FeO	0.37	0.38	0.18	0.29	0.41	0.52	0.21	0.26	0.47	0.39	0.52	0.45	0.53
CaO	15.31	12.32	10.75	7.02	12.08	12.47	7.99	10.57	12.64	13.20	12.34	12.92	12.69
Na_2O	2.84	4.10	5.24	7.35	4.47	4.14	6.58	5.30	4.17	3.96	4.12	4.10	4.09
K_2O	0.09	0.19	0.17	0.45	0.19	0.16	0.35	0.27	0.15	0.15	0.19	0.16	0.17
BaO	0.00	0.00	0.00	0.00	0.00	0.00	0.00	0.00	0.00	0.00	0.00	0.00	0.00
Total	99.56	99.23	99.56	100.46	99.76	98.92	99.44	99.63	99.05	99.18	99.25	99.85	98.89
Si	8.79	9.43	9.83	10.82	9.54	9.41	10.44	9.88	9.36	9.27	9.48	9.38	9.33
Al	6.87	6.39	6.13	5.41	6.35	6.28	5.64	6.07	6.34	6.41	6.29	6.45	6.34
Fe^{2+}	0.06	0.06	0.03	0.04	0.06	0.08	0.03	0.04	0.07	0.06	0.08	0.07	0.08
Ca	2.96	2.38	2.08	1.36	2.34	2.41	1.55	2.04	2.45	2.55	2.39	2.50	2.46
Na	0.99	1.44	1.84	2.57	1.56	1.45	2.30	1.86	1.46	1.39	1.44	1.44	1.43
K	0.02	0.04	0.04	0.10	0.04	0.04	0.08	0.06	0.04	0.04	0.04	0.04	0.04
Ba	0.00	0.00	0.00	0.00	0.00	0.00	0.00	0.00	0.00	0.00	0.00	0.00	0.00
Total	19.69	19.74	19.94	20.31	19.89	19.67	20.04	19.96	19.71	19.72	19.73	19.87	19.67
An	75	62	53	33	59	62	39	52	62	64	62	63	63
Ab	25	37	46	64	40	37	59	47	37	35	37	36	36
Or	0	1	1	3	1	1	2	1	1	1	1	1	1
Total	100	100	100	100	100	100	100	100	100	100	100	100	100

The formula was calculated on the basis of 32 oxygens. Fe^{2+} was taken as total Fe. pl: plagioclase; pheno: phenocrysts; mid.: middle.

Appendix D. (Continued).

Sample	Po-6	Po-6	Po-6	Po-17	Po-17	Po-17	Po-21	Po-21	Po-21	Po-21	Po-31	Po-31	Po-31	Po-31	Po-31	Po-31
Mineral	c2	c3	c7	c2	c5	c5	c1	c4	c9	c11	c1	c2	c3	c3	c4	c5
	pl	pl	pl	pl	pl	pl	pl	pl	pl	pl	pl	pl	pl	pl	pl	pl
	mic	mic	mic	mic	mic2	mic3	mic1	mic	mic4	mic	mic1	mic	mic3	mic4	mic5	mic6
SiO_2	55.72	52.95	54.06	56.36	53.53	52.91	51.08	54.38	51.63	51.00	53.02	63.20	53.27	52.13	59.49	52.55
Al_2O_3	27.34	28.99	28.52	26.31	28.68	29.13	30.70	28.18	30.44	30.23	28.57	22.36	28.78	30.39	24.82	29.73
FeO	1.28	0.93	0.98	1.20	0.94	0.88	0.68	0.67	0.66	0.63	0.63	0.40	0.64	0.62	0.59	0.52
CaO	9.99	12.41	11.55	9.14	11.45	11.80	13.35	11.02	13.42	13.68	11.48	3.27	11.45	12.40	6.34	12.04
Na_2O	5.61	4.32	4.67	5.78	4.81	4.36	3.91	5.29	4.00	3.85	4.76	7.45	4.56	4.10	6.95	4.50
K_2O	0.46	0.28	0.34	0.68	0.43	0.40	0.15	0.29	0.21	0.15	0.38	3.10	0.34	0.27	1.30	0.32
BaO	0.00	0.00	0.00	0.00	0.00	0.00	0.00	0.00	0.00	0.00	0.00	0.00	0.00	0.00	0.00	0.00
Total	100.40	99.89	100.12	99.47	99.84	99.48	99.88	99.84	100.35	99.53	98.85	99.76	99.05	99.91	99.50	99.65
Si	10.06	9.65	9.80	10.24	9.75	9.67	9.33	9.87	9.39	9.36	9.74	11.30	9.75	9.48	10.71	9.58
Al	5.82	6.23	6.09	5.63	6.15	6.27	6.61	6.03	6.52	6.54	6.18	4.71	6.21	6.51	5.27	6.39
Fe^{2+}	0.19	0.14	0.15	0.18	0.14	0.13	0.10	0.10	0.10	0.10	0.10	0.06	0.10	0.09	0.09	0.08
Ca	1.93	2.42	2.24	1.78	2.23	2.31	2.61	2.14	2.61	2.69	2.26	0.63	2.25	2.42	1.22	2.35
Na	1.96	1.53	1.64	2.04	1.70	1.54	1.39	1.86	1.41	1.37	1.70	2.58	1.62	1.45	2.43	1.59
K	0.11	0.07	0.08	0.16	0.10	0.09	0.03	0.07	0.05	0.03	0.09	0.71	0.08	0.06	0.30	0.07
Ba	0.00	0.00	0.00	0.00	0.00	0.00	0.00	0.00	0.00	0.00	0.00	0.00	0.00	0.00	0.00	0.00
Total	20.07	20.03	20.01	20.04	20.07	20.02	20.08	20.08	20.08	20.08	20.06	19.99	20.00	20.02	20.02	20.06
An	48	60	57	45	55	59	65	52	64	66	56	16	57	62	31	58
Ab	49	38	41	51	42	39	35	46	35	33	42	66	41	37	62	40
Or	2	2	2	4	3	2	1	2	1	1	2	18	2	1	7	2
Total	100	100	100	100	100	100	100	100	100	100	100	100	100	100	100	100

The formula was calculated on the basis of 32 oxygens. Fe^{2+} was taken as total Fe. pl: plagioclase; mic: microlite.

Appendix D. (Continued).

Sample	Po-31	Po-35	Po-35	Po-35	Po-35
Mineral	c6	c1	c1	c6	c9
	pl	pl	pl	pl	pl
	mic7	mic1	mic2	mic1	mic
SiO_2	52.44	52.36	55.91	52.89	53.91
Al_2O_3	30.19	29.56	27.15	29.10	28.36
FeO	0.51	0.47	0.41	0.47	0.51
CaO	12.57	12.67	9.73	11.74	10.95
Na_2O	4.37	4.34	5.74	4.55	5.08
K_2O	0.27	0.17	0.29	0.19	0.25
BaO	0.00	0.00	0.00	0.00	0.00
Total	100.34	99.57	99.23	98.94	99.05
Si	9.50	9.56	10.15	9.69	9.85
Al	6.45	6.36	5.81	6.28	6.11
Fe^{2+}	0.08	0.07	0.06	0.07	0.08
Ca	2.44	2.48	1.89	2.30	2.14
Na	1.54	1.54	2.02	1.62	1.80
K	0.06	0.04	0.07	0.04	0.06
Ba	0.00	0.00	0.00	0.00	0.00
Total	20.07	20.05	19.99	20.00	20.03
An	60	61	48	58	54
Ab	38	38	51	41	45
Or	2	1	2	1	1
Total	100	100	100	100	100

The formula was calculated on the basis of 32 oxygens. Fe^{2+} was taken as total Fe. pl: plagioclase; mic: microlite.

Appendix E.

Electron microprobe analysis results of hornblende phenocrysts from Late Miocene basic volcanic rocks.

Sample	Po-35	Po-35	Po-35	Po-35	Po-35	Po-35	Po-35	Po-35	Po-35	Po-35	Po-35	Po-35	Po-35	Po-35	Po-35	Po-35	Po-35	Po-35	Po-35	Po-35
Mineral	c1	c2	c2	c3	c3	c4	c4	c4	c6	c6	c6	c6	c7	c7	c10	c10	c10	c10	c11	
	hbl-1	hbl-1	hbl-1	hbl-1	hbl-1	hbl-1	hbl-1	hbl-2	hbl-1	hbl-1	hbl-2	hbl-3	hbl-1	hbl-1	hbl-1	hbl-1	hbl-2	hbl-2	hbl-1	
	pheno	pheno	pheno	pheno	pheno	pheno	pheno	pheno	pheno	pheno	pheno	pheno	pheno	pheno	pheno	pheno	pheno	pheno	pheno	
	core	core	rim	core	rim	core	rim	core	core	rim	core	core	core	rim	core	rim	core	rim	core	
SiO_2	42.27	42.26	44.12	41.35	41.56	41.25	42.58	42.66	40.78	40.57	41.35	41.36	43.43	43.59	41.84	42.49	41.54	41.64	42.80	
TiO_2	2.77	2.94	1.88	3.48	2.32	3.41	2.22	3.34	3.47	3.26	3.11	3.23	2.52	2.05	3.43	3.14	3.21	3.45	2.83	
Al_2O_3	13.22	11.54	10.49	12.56	12.17	13.33	12.09	11.79	12.71	12.55	12.87	12.79	10.49	10.79	12.17	11.95	12.29	12.17	12.17	
Cr_2O_3	0.00	0.00	0.00	0.00	0.00	0.00	0.00	0.00	0.00	0.00	0.00	0.00	0.02	0.00	0.00	0.01	0.00	0.00	0.00	
FeO	11.96	12.98	12.46	13.06	15.71	11.43	12.83	12.12	13.39	13.53	13.21	12.69	13.15	13.74	11.72	11.34	11.63	12.13	13.29	
MnO	0.15	0.17	0.19	0.16	0.31	0.11	0.20	0.11	0.13	0.15	0.15	0.16	0.27	0.36	0.15	0.13	0.09	0.11	0.15	
MgO	13.86	13.33	14.31	13.15	12.56	13.94	13.53	13.63	12.76	12.51	12.69	13.17	14.10	14.08	13.65	14.01	13.78	13.42	12.97	
CaO	10.68	11.34	11.34	11.17	10.60	11.42	11.26	10.87	10.83	11.80	10.77	10.87	10.71	10.63	11.05	11.15	11.24	11.22	10.67	
Na_2O	2.65	2.27	1.99	2.39	2.38	2.51	2.34	2.56	2.29	2.19	2.38	2.45	2.10	2.28	2.44	2.43	2.39	2.36	2.21	
K_2O	0.42	0.58	0.50	0.62	0.64	0.54	0.54	0.56	0.59	0.55	0.54	0.56	0.51	0.55	0.59	0.53	0.55	0.57	0.56	
Total	97.99	97.41	97.27	97.93	98.26	97.93	97.60	97.64	96.95	97.11	97.08	97.29	97.31	98.06	97.03	97.19	96.74	97.09	97.65	
Si	6.09	6.19	6.43	6.03	6.10	5.96	6.20	6.18	6.01	6.00	6.07	6.05	6.35	6.37	6.12	6.21	6.07	6.09	6.26	
$Al^{[IV]}$	1.91	1.81	1.57	1.97	1.90	2.04	1.80	1.82	1.99	2.00	1.93	1.95	1.65	1.63	1.88	1.79	1.93	1.91	1.74	
T	8.00	8.00	8.00	8.00	8.00	8.00	8.00	8.00	8.00	8.00	8.00	8.00	8.00	8.00	8.00	8.00	8.00	8.00	8.00	
$Al^{[VI]}$	0.33	0.18	0.23	0.18	0.21	0.24	0.28	0.20	0.22	0.18	0.29	0.25	0.16	0.23	0.21	0.27	0.19	0.18	0.35	
Ti	0.30	0.32	0.21	0.38	0.26	0.37	0.24	0.36	0.38	0.36	0.34	0.36	0.28	0.22	0.38	0.34	0.35	0.38	0.31	
Cr	0.00	0.00	0.00	0.00	0.00	0.00	0.00	0.00	0.00	0.00	0.00	0.00	0.00	0.00	0.00	0.00	0.00	0.00	0.00	
Fe^{3+}	0.23	0.06	0.30	0.12	0.64	0.03	0.17	0.00	0.27	0.00	0.19	0.17	0.52	0.86	0.06	0.25	0.00	0.00	0.47	
Fe^{2+}	1.21	1.52	1.21	1.46	1.27	1.35	1.39	1.47	1.37	1.67	1.43	1.38	1.07	0.80	1.36	1.12	1.42	1.48	1.14	
Mn	0.02	0.02	0.02	0.02	0.04	0.01	0.02	0.01	0.02	0.02	0.02	0.02	0.03	0.04	0.02	0.02	0.01	0.01	0.02	
Mg	2.98	2.91	3.11	2.86	2.75	3.01	2.94	2.95	2.80	2.76	2.78	2.87	3.07	3.07	2.98	3.05	3.00	2.93	2.83	
C	5.06	5.02	5.08	5.03	5.16	5.01	5.04	4.99	5.07	5.00	5.05	5.04	5.13	5.23	5.00	5.06	4.98	4.99	5.12	
Ca	1.64	1.78	1.76	1.74	1.64	1.77	1.75	1.69	1.70	1.87	1.69	1.70	1.66	1.65	1.71	1.73	1.76	1.76	1.65	
Na	0.35	0.22	0.23	0.26	0.33	0.23	0.24	0.31	0.29	0.13	0.31	0.30	0.32	0.34	0.27	0.25	0.24	0.24	0.33	
B	1.99	2.00	1.99	2.00	1.98	2.00	1.99	2.00	1.99	2.00	1.99	1.99	1.98	1.98	1.98	1.98	2.00	2.00	1.98	
Na	1.12	1.07	0.89	1.09	1.00	1.17	1.07	1.13	1.01	1.13	1.04	1.08	0.85	0.94	1.10	1.11	1.12	1.10	0.91	
K	0.08	0.11	0.09	0.11	0.12	0.10	0.10	0.10	0.11	0.10	0.10	0.10	0.09	0.10	0.11	0.10	0.10	0.11	0.10	
A	1.20	1.17	0.98	1.21	1.12	1.27	1.17	1.23	1.12	1.23	1.14	1.19	0.95	1.04	1.20	1.21	1.22	1.20	1.01	
$Al^{[T]}$	2.24	1.99	1.80	2.16	2.11	2.27	2.08	2.01	2.21	2.19	2.23	2.20	1.81	1.86	2.10	2.06	2.12	2.10	2.10	
Mg#	0.71	0.66	0.72	0.66	0.68	0.69	0.68	0.67	0.67	0.62	0.66	0.67	0.74	0.79	0.68	0.73	0.68	0.66	0.71	

Mg#=Mg/(Mg+Fe2+). The formula was calculated on the basis of 23 oxygens. hbl: hornblende; pheno: phenocrysts.

Appendix F.

Electron microprobe analysis results of Fe-Ti oxide mineral from Late Miocene basic volcanic rocks.

Sample	Po-6	Po-6	Po-6	Po-6	Po-6	Po-6	Po-6	Po-6	Po-6	Po-6	Po-6	Po-6	Po-17	Po-17	Po-17	Po-17	Po-17	Po-17
Mineral	c1	c1	c4	c5	c6	c7	c11	c11	c11	c11	c11	c11	c1	c3	c3	c3	c7	c8
	opq1	opq2	opq3	opq4	opq5	opq5	opq6	opq7	opq8	opq9	opq10	opq11	opq1	opq2	opq3	opq4	opq5	opq 1
SiO_2	0.49	0.59	0.13	0.29	0.33	0.65	0.33	0.12	0.41	0.36	0.19	0.22	0.11	0.05	0.07	0.07	0.69	0.06
TiO_2	11.61	11.88	12.28	11.56	13.31	12.26	11.47	11.88	12.30	11.93	11.37	11.72	8.66	8.07	8.49	7.89	8.92	2.64
Al_2O_3	1.53	1.62	1.79	1.69	1.47	1.14	1.44	1.09	1.53	1.90	1.49	1.71	2.41	2.51	2.42	2.80	2.34	5.60
Cr_2O_3	0.00	0.00	0.00	0.02	0.04	0.06	0.00	0.01	0.00	0.01	0.00	0.02	0.48	0.91	0.70	0.71	0.45	16.88
FeO	76.78	76.31	76.12	75.35	74.05	74.59	75.62	76.25	75.68	74.39	76.72	75.13	78.04	79.82	79.48	79.18	77.74	63.86
MnO	0.54	0.54	0.51	0.52	0.51	0.55	0.54	0.48	0.42	0.53	0.39	0.38	0.59	0.53	0.58	0.54	0.59	0.34
MgO	0.74	0.61	0.85	0.81	1.04	0.62	0.80	0.70	0.78	0.85	0.91	0.54	3.45	3.23	3.49	3.99	3.51	6.27
CaO	0.17	0.14	0.06	0.11	0.09	0.22	0.13	0.06	0.07	0.13	0.14	0.09	0.22	0.08	0.12	0.06	0.20	0.02
Total	91.85	91.69	91.74	90.36	90.85	90.08	90.33	90.59	91.19	90.09	91.22	89.80	93.96	95.21	95.35	95.24	94.44	95.66
Si	0.15	0.18	0.04	0.09	0.10	0.21	0.10	0.04	0.13	0.11	0.06	0.07	0.03	0.02	0.02	0.02	0.20	0.02
Ti	2.72	2.79	2.88	2.75	3.16	2.94	2.74	2.84	2.91	2.85	2.68	2.82	1.93	1.78	1.87	1.72	1.98	0.56
Al	0.56	0.60	0.66	0.63	0.55	0.43	0.54	0.41	0.57	0.71	0.55	0.64	0.84	0.87	0.83	0.96	0.81	1.86
Cr	0.00	0.00	0.00	0.01	0.01	0.02	0.00	0.00	0.00	0.00	0.00	0.01	0.11	0.21	0.16	0.16	0.11	3.77
Fe^{2+}	10.33	10.50	10.37	10.29	10.61	10.63	10.27	10.40	10.54	10.37	10.17	10.50	8.22	8.23	8.19	7.86	8.43	5.85
Fe^{3+}	9.69	9.45	9.50	9.67	8.92	9.26	9.78	9.84	9.36	9.37	9.96	9.58	11.12	11.33	11.23	11.39	10.72	9.22
Mn	0.14	0.14	0.14	0.14	0.13	0.15	0.15	0.13	0.11	0.14	0.10	0.10	0.15	0.13	0.14	0.13	0.15	0.08
Mg	0.34	0.29	0.40	0.38	0.49	0.29	0.38	0.33	0.37	0.40	0.43	0.26	1.52	1.41	1.52	1.73	1.54	2.64
Ca	0.06	0.05	0.02	0.04	0.03	0.07	0.04	0.02	0.02	0.04	0.05	0.03	0.07	0.02	0.04	0.02	0.06	0.00
Total	24.00	24.00	24.00	24.00	24.00	24.00	24.00	24.00	24.00	24.00	24.00	24.00	24.00	24.00	24.00	24.00	24.00	24.00
Usp	0.61	0.62	0.63	0.62	0.66	0.64	0.61	0.63	0.63	0.63	0.61	0.62	0.50	0.47	0.48	0.46	0.50	0.19
İlmenite																		

The Fe^{2+} and Fe^{3+} proportions were calculated stoichiometrically. The Usp ratio was calculated according to Lindsley and Spencer (1982). Mg#=Mg/(Mg+Fe2+). The formula was calculated on the basis of 32 oxygens. opq: opaque mineral.

Appendix F. (Continued).

Sample	Po-21	Po-21	Po-21	Po-21	Po-21	Po-21	Po-21	Po-31	Po-31	Po-31	Po-31	Po-31	Po-31	Po-31	Po-31	Po-35	Po-35	Po-35	Po-35	Po-35
Mineral	c2	c5	c6	c7	c8	c11	c12	c1	c1	c1	c2	c3	c4	c5	c6	c6	c7	c7	c8	c7
	opq1	opq2	opq3	opq 4	opq1	opq5	opq6	opq1	opq2	opq2	opq3	opq4	opq5	opq 6	opq7	opq1	opq2	opq3	opq4	opq-mic
SiO_2	0.25	0.07	0.03	0.01	0.07	0.10	0.44	0.04	0.06	0.05	0.05	0.01	0.03	0.04	0.02	0.06	0.08	0.07	0.05	0.10
TiO_2	23.57	24.06	51.51	51.09	2.93	24.28	49.88	16.90	18.60	15.95	18.39	18.87	18.14	18.00	18.17	1.44	30.05	0.66	16.92	31.19
Al_2O_3	1.00	0.83	0.05	0.08	14.30	1.18	0.29	2.42	2.28	3.32	2.35	2.45	2.31	2.37	2.62	1.26	1.51	0.61	0.46	0.40
Cr_2O_3	0.00	0.04	0.00	0.00	33.51	0.02	0.01	0.72	0.27	1.78	0.29	0.21	0.34	0.39	0.29	0.02	0.07	0.00	0.00	0.00
FeO	68.15	69.52	44.30	45.86	42.76	69.04	44.07	72.53	70.77	71.14	69.76	70.65	71.40	70.93	70.42	86.58	56.89	88.35	70.88	53.88
MnO	0.63	0.54	0.60	0.61	0.39	0.60	0.57	0.67	0.65	0.58	0.63	0.70	0.68	0.73	0.75	0.17	0.34	0.94	0.46	0.39
MgO	2.42	2.25	3.20	2.90	4.50	2.87	3.10	3.64	4.11	3.55	4.14	3.94	4.04	4.00	4.26	0.82	2.58	2.91	1.08	3.44
CaO	0.79	0.07	0.05	0.10	0.01	0.05	1.00	0.00	0.03	0.20	0.05	0.01	0.09	0.09	0.01	0.09	0.07	0.06	0.20	0.21
Total	96.81	97.39	99.75	100.64	98.47	98.12	99.36	96.93	96.78	96.58	95.66	96.83	97.02	96.55	96.54	90.44	91.59	93.60	90.05	89.62
Si	0.07	0.02	0.01	0.00	0.02	0.03	0.13	0.01	0.02	0.02	0.02	0.00	0.01	0.01	0.01	0.02	0.02	0.02	0.02	0.03
Ti	5.24	5.35	11.45	11.27	0.60	5.32	11.07	3.68	4.05	3.48	4.05	4.11	3.94	3.93	3.96	0.34	7.11	0.15	4.08	7.53
Al	0.35	0.29	0.02	0.03	4.57	0.40	0.10	0.83	0.78	1.13	0.81	0.84	0.79	0.81	0.89	0.47	0.56	0.21	0.17	0.15
Cr	0.00	0.01	0.00	0.00	7.19	0.00	0.00	0.17	0.06	0.41	0.07	0.05	0.08	0.09	0.07	0.01	0.02	0.00	0.00	0.00
Fe^{2+}	11.84	12.22	17.88	17.82	6.71	11.94	17.38	9.96	10.13	9.75	10.09	10.24	10.02	10.00	9.94	7.90	13.81	6.62	11.39	13.74
Fe^{3+}	5.02	4.96	-6.93	-6.57	3.00	4.89	-6.50	7.62	7.02	7.48	6.99	6.88	7.24	7.22	7.11	14.81	1.15	15.45	7.63	0.72
Mn	0.16	0.14	0.15	0.15	0.09	0.15	0.14	0.17	0.16	0.14	0.16	0.17	0.17	0.18	0.18	0.05	0.09	0.24	0.13	0.11
Mg	1.07	0.99	1.41	1.27	1.82	1.25	1.36	1.57	1.77	1.53	1.81	1.70	1.74	1.73	1.84	0.38	1.21	1.30	0.52	1.64
Ca	0.25	0.02	0.02	0.03	0.00	0.02	0.32	0.00	0.01	0.06	0.02	0.00	0.03	0.03	0.00	0.03	0.02	0.02	0.07	0.07
Total	24.00	24.00	24.00	24.00	24.00	24.00	24.00	24.00	24.00	24.00	24.00	24.00	24.00	24.00	24.00	24.00	24.00	24.00	24.00	24.00
Usp	0.87	0.86	1.44	1.42	0.20	0.86	1.42	0.73	0.76	0.71	0.76	0.77	0.75	0.75	0.75	0.12	0.96	0.05	0.77	0.99
İlmenite			0.96	0.94			0.94													

The Fe^{2+} and Fe^{3+} proportions were calculated stoichiometrically. The Usp ratio was calculated according to Lindsley and Spencer (1982). Mg#=Mg/(Mg+Fe2+). The formula was calculated on the basis of 32 oxygens. opq: opaque mineral.